CHARACTERISATION OF SURFACES MODIFIED WITH PHTHALOCYANINES THROUGH CLICK CHEMISTRY FOR APPLICATIONS IN ELECTROCHEMICAL SENSING

A thesis submitted in fulfilment of the requirements for the degree of

MASTER OF SCIENCE

of

RHODES UNIVERSITY

by

CHARLES ST JOHN NQWABUKO O'DONOGHUE

Supervisor: **Dist. Prof. T. Nyokong**

April 2017

ABSTRACT

One form of surface modification was primarily investigated in this work on glassy carbon electrodes. The form of modification is comprised of a series of steps in which electrografting is first applied to the glassy carbon surface, which is then followed up with click chemistry to ultimately immobilise a phthalocyanine onto the surface. The modified glassy carbon electrodes and surfaces were characterised with a combination of scanning electrochemical microscopy, X-ray photoelectron spectroscopy and various electrochemical methods.

In this work, three alkyne substituted phthalocyanines were used. Two novel phthalocyanines, with nickel and cobalt metal centres, were studied alongside a manganese phthalocyanine reported in literature. Each of the three phthalocyanines was modified at the peripheral position with a 1-hexyne group, via a glycosidic bond, yielding the terminal alkyne groups that were used for subsequent click reactions. *In situ* diazotisation was used to graft 4-azidoaniline groups to the surface of the glassy carbon electrode. The azide bearing 4-azidoaniline groups were thus used to anchor the tetra substituted phthalocyanines to the surface of the electrodes. This method yielded successful modification of the electrodes and lead to their application in sensing studies. The modified electrodes were primarily used to catalyse the common agricultural oxidising agent hydrazine.

ACKNOWLEDGEMENTS

I would like to start by thanking my supervisor, Prof. T. Nyokong, who I have come to affectionately know as 'Prof'. Prof first caught my attention in my third year when I was to do an internship in her acclaimed laboratory, S22. I was drawn to the laboratory as it held promises of taking me into the world of nanotechnology. Little did I know how I lucky I would become, when following the internship, Prof asked me back for Honours. She took me under her wing and promised me that she would support me not only as a supervisor but with bursaries and publications too. She has been a pillar in my journey from clueless third year, to a slightly less clueless masters student. Prof has shown me how to present, how to write, how to fight procrastination and ultimately to grow as a young scientist. If I could thank you enough, I would be thrilled, for I know not how. I only hope you continue to grow your legacy and change the world.

I would like to extend my thanks to Ms. Gail Cobus for all of her help in keeping my financial support in order, for always being down the hall for any questions, for always being so willing to go on field days and get out of Grahamstown and have some fun. Thank you.

I would like to acknowledge the Goddard Family for their financial support that carried me from Honours into M.Sc. I would to thank the DST/Mintek Centre for Nanotechnology Innovation (CNI), for carrying me through my final year of M.Sc. This work was supported by the DST/NRF South African Research Chairs Initiative for Professor of Medicinal Chemistry and Nanotechnology as well as Rhodes University.

I would like to send out my thanks to the Rhodes University Rowing Club, another family I have been a part of ever since I came to Rhodes. I am grateful for how the sport and club has carried me through hard and fun times throughout my academic career.

I extend my thanks to my friends/colleagues current and past from F26, without you the many hours spent staring at a screen hoping electrodes were behaving would not have been the same. I also send out my thanks to our 'mother' lab, S22, for which without the members of, I would not have learnt how to be a chemist.

I want to thank my friends, for meeting me at tea when nobody else was around and always being willing to listen to one my wild ideas. Particularly Munya, Ntsika, and Laura.

I wish to send out thanks to Cathy and Anton Vorster for looking after me in their upstairs flat.

I give thanks to Mark, Anne and Amy Harris, for welcoming me into their home and always being there to support me, be it when in need of a second home, or simply a vehicle to go to the airport. I cannot express my gratitude for your support and hospitality throughout my Rhodes career.

To Jess: we have been through this together, right from first year and now out into the big, wide world. I thank you for always being by my side, for all the rowing escapes, help with arithmetic and unwavering support.

Finally, thank you to my mum, Lyzzie, and to my sister, Sophie. I could not have begun this journey into higher education without you and I could not have been more believed in than by you two. To both of you thank you for everything.

CONTENTS

LIST OF ABBREVIATIONS

ACN	Acetonitrile
AFM	Atomic Force Microscopy
a.u.	Arbitrary Unit
CA	Chronoamperometry
CE	Counter Electrode
CV	Cyclic voltammetry/voltammogram
DMF	N,N-dimethylformamide
DMSO	Dimethylsulfoxide
EIS	Electrochemical Impedance Spectroscopy
GCE	Glassy carbon electrode
grafted-GCE	Electrografted GCE
2-clicked-GCE	GCE with clicked manganese phthalocyanine
3-clicked-GCE	GCE with clicked cobalt phthalocyanine
4-clicked-GCE	GCE with clicked nickel phthalocyanine
HOMO	Highest occupied molecular orbital
IR	Infrared
LoD	Limit of detection
LUMO	Lowest unoccupied molecular orbital
MALDI-TOF	Matrix Assisted Laser Desorption/Ionisation – Time of Flight
MPc	Metallophthalocyanine
Pc	Phthalocyanine
RDS	Rate determining step
RE	Reference electrode
Redox	Reduction/oxidation
SECM	Scanning electrochemical microscopy
$TBABF_4$	Tetrabutylammonium tetrafluoroborate
UME	Ultramicroelectrode
UV-vis	Ultraviolet-visible
WE	Working electrode
XPS	X-ray photoelectron spectroscopy

LIST OF SYMBOLS

α	Non-peripheral position
β	Peripheral position
ε	Extinction coefficient
θ	Phase shift
λ_Q	Wavelength of the maximum absorbance of the Q band
A	Absorbance/real area of the electrode
a	Radius
C	Concentration
D	Diffusion coefficient
d	Distance
e^-	Electron
ΔE	Peak to peak potential separation
E_p	Peak potential
F	Faraday's constant
I	Current
I_P	Peak Current
M	Molar concentration
n	Number of electrons transferred
R	Universal gas constant
R_{CT}	Charge transfer resistance
rt	Room tempertaure
T	Temperature
ν	Scan rate
V	Volts
Z'	Real impedance component
Z''	Imaginary impedance component

CHAPTER 1

INTRODUCTION

CHAPTER 1 INTRODUCTION

Surface modification is becoming an increasingly popular area of research due to its applications in fields such as renewable energy, anti-pollution systems such as water purification and electrochemical sensing. This work will focus on the use of surface modification to generate electrodes capable of efficient electrochemical sensing. However, the techniques employed here can be applied to other areas and materials. There are several well-known methods for the modification of electrode surfaces. The choice of modification method depends on the type of electrode, the nature of the molecule or substance to be immobilised onto the surface and, finally, the intended application of the modified electrode.

The compounds (phthalocyanines in this case) that have been used to modify surfaces will be discussed. Following that, the attachment method and characterisation techniques employed are outlined.

1.1 Background on metallophthalocyanines (Pcs)

1.1.1 General properties and applications

Porphyrin complexes have generated interest due to their redox and photophysical properties. Phthalocyanines (Pcs) are a subset of molecules from the main porphyrinoid set. They differ from the well-known porphyrin due to their possession of aza-nitrogens and four benzene rings (Fig. 1.1) [1–4]. These structural differences cause beneficial changes such as improved thermal stability and lower reactivity, which tends to improve reliability and has led to their development into catalysts [5–14].

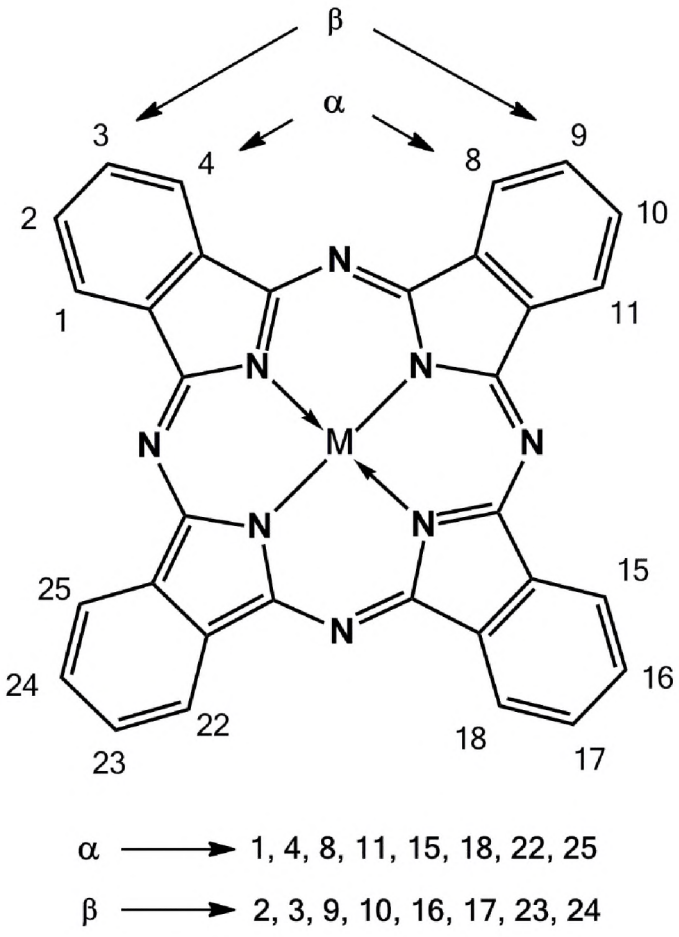

Figure 1.1. Structure and naming convention for a phthalocyanine.

The phthalocyanine's macrocyclic structure has an 18π electron system that makes them aromatic and thus, able to be studied under molecular orbital theory. This aromaticity is the basis for the compounds' electronic transitions, which are significant in explaining their redox and photophysical behaviour. Their redox behaviour is generally governed by the nature of

the substituents. Electron withdrawing groups, for example, cause electron density to be shifted out of the 18π electron system, thereby making oxidation difficult. The opposite is observed if the peripheral substituents are electron donating. There are many simple methods by which Pcs can have their properties modified and this has given rise to a diverse range of Pcs, which has contributed to their popularity in research. What is most apparent is that Pcs can be made to suit specific applications by designing them to exhibit particular properties. This is typically done by varying the substituents at the α- and β-positions, and by changing the central metal. Based on the central metal and substituents, Pcs have been used in areas ranging from optics and imaging to the treatment of cancer with photodynamic therapy [1,13,14].

The central metals that have been shown to be most effective in electrochemistry are the d-group metals, namely manganese, iron, cobalt and nickel. These metals are electroactive within metallophthalocyanine (MPc). The periphery of the Pc can then be modified to facilitate attachment of the MPcs to electrodes. While the electrochemical properties of alkyne substituted FePc have been investigated before [15], this work considers the properties of the corresponding manganese, cobalt and nickel phthalocyanines covalently attached to electrode surfaces via the 'click' reaction.

1.1.2 Metallophthalocyanine (MPc) synthesis

Many methods have been developed to synthesise unsubstituted MPcs but the most common is the template reaction of a phthalonitrile with a metal salt [16]. Phthalic anhydride, 1, 3-diiminoisoindoline, phthalamide or phthalic acid are among some of the other starting the materials than can be used to synthesise the Pc [16]. The template reaction requires the reflux of the phthalonitrile and metal salt in a suitable solvent, in the presence of either a catalyst or a base. If an unmetallated Pc is desired then the reaction can be carried out without the metal salt. This work focusses on metallated Pcs.

Pcs can be tetra-, octa-, dodeca- or hexadeca-substituted, depending on the phthalonitrile used (Scheme 1.1). The dodeca-substituted Pc is highly uncommon. It is also important to note that in the synthesis of the tetra-substituted there are many isomers that are not shown in Scheme 1.1 but are typically represented by floating bonds for three out of the four

substituents [17]. Furthermore, the properties of Pcs may differ depending on whether substitution occurs at the α or β positions.

This work will focus on the synthesis, characterisation and application of the β tetra-substituted Pc.

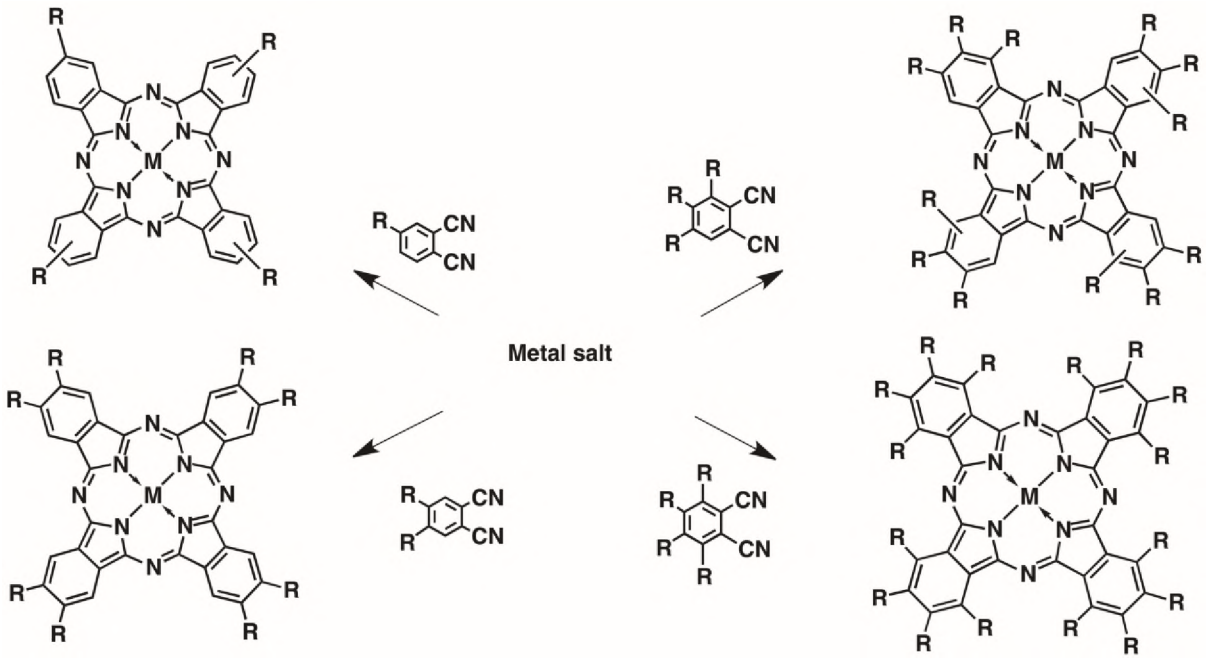

Scheme 1.1. All routes to four different Pcs with associated phthalonitriles, where R = alkyl, aryl, halogen and substituent of choice, in general.

1.1.3 Electronic spectra of Pcs

Spectral properties of metallophthalocyanines and other tetraazaporphyrins are governed mainly by the Q band, which originates from the π-π* transitions within the ring. The position and intensity of the Q band is an important consideration when tailoring new phthalocyanine derivatives for specific applications. Aggregation, the nature of the central metal, π conjugation, symmetry of the molecule, and axial, peripheral or non-peripheral substitutions affect the spectra and hence the properties of the phthalocyanine molecule [18]. Pcs have two characteristic absorbance bands (Q and Soret/B band) [2,3]. These arise due to electronic transitions the molecules exhibit, which can be explained by Gouterman's four orbital model (Fig. 1.2(A)) [19]. The Pc Q band is typically seen between 600– 800 nm but is not restricted to this range, with some Pcs having been modified to show Q band absorption in IR region (over 1000 nm) [20]. The B band tends to absorb in the range of 300–400 nm but, once again,

can be shifted with appropriate modifications, but only slightly. The Q band is characteristically more intense than the B band, as shown in Fig. 1.2(B) [3]. Molecular orbital diagrams are often used to schematically depict how these transitions occur by illustrating the transitions from one energy level to another (Fig. 1.2(C)) [3]. The Q band arises from electron transitions from the a_{1u} energy level, which is the highest occupied molecular orbital (HOMO), to the e_g level, which is the lowest unoccupied molecular orbital (LUMO). The B band, which is made up of two transitions, is generated by the transition from a_{2u} to e_g forming the B_1 band; and the transition of b_{2u} to e_g, forming the B_2 band.

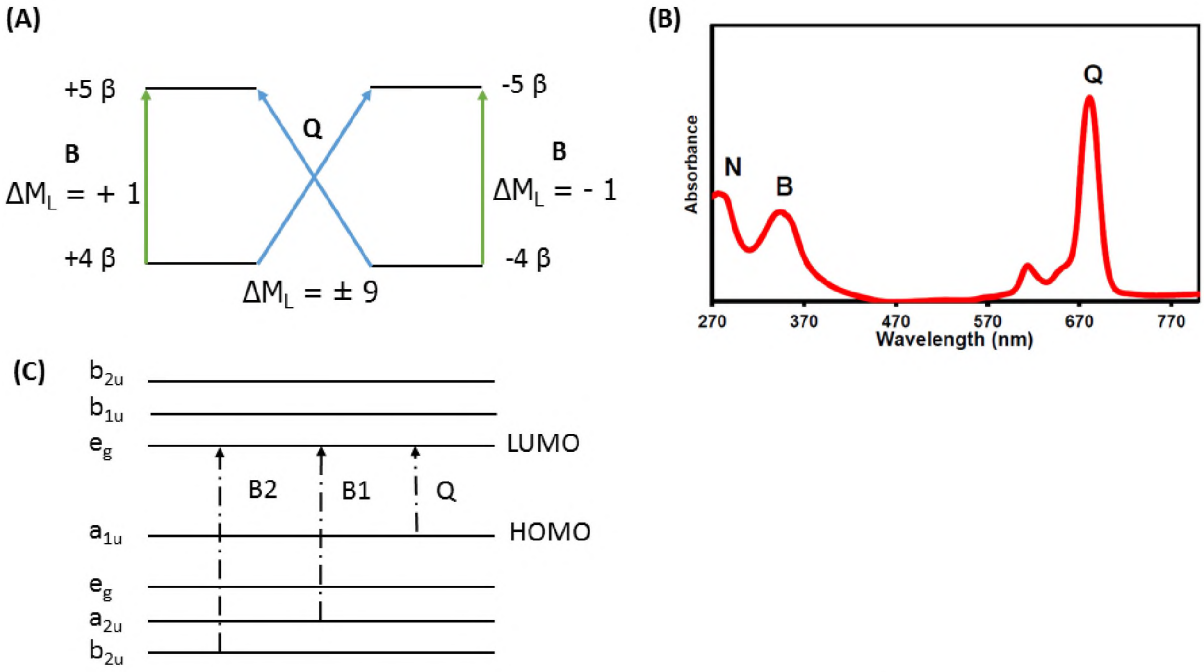

Figure 1.2. (A) Molecular orbital diagram of electronic transitions that form Pc UV-vis absorption spectrum – the Gouterman Four Orbital Model. (B) A typical Pc UV-vis spectrum, Q and B bands labelled. (C) The electronic transitions that generate the Pc spectra based on the Gouterman's model.

1.2 Modification approaches

In this work, electrochemistry was used – in the form of electrografting – to modify an electrode directly. The drop dry method of adsorption was also employed in this work. Both methods are described below.

1.2.1 Electrografting with diazonium salts

Electrochemical or chemical reduction can be used to covalently bond a molecule to a conductive surface; the technique is known as grafting. Although the majority of work done using grafting involves carbon electrodes, the technique is not limited to carbon-based electrodes. This technique is very versatile as a result of being applicable to effectively any surface that is conductive [21–24]. This technique was first shown by Delamar *et al.* in 1992, who demonstrated that the electrochemical reduction of diazonium salts results in their bonding directly to a carbon surface [21]. Scheme 1.2 shows how electrografting takes place at a carbon surface, namely a glassy carbon electrode, and how nitrogen is produced as a by-product [21,22].

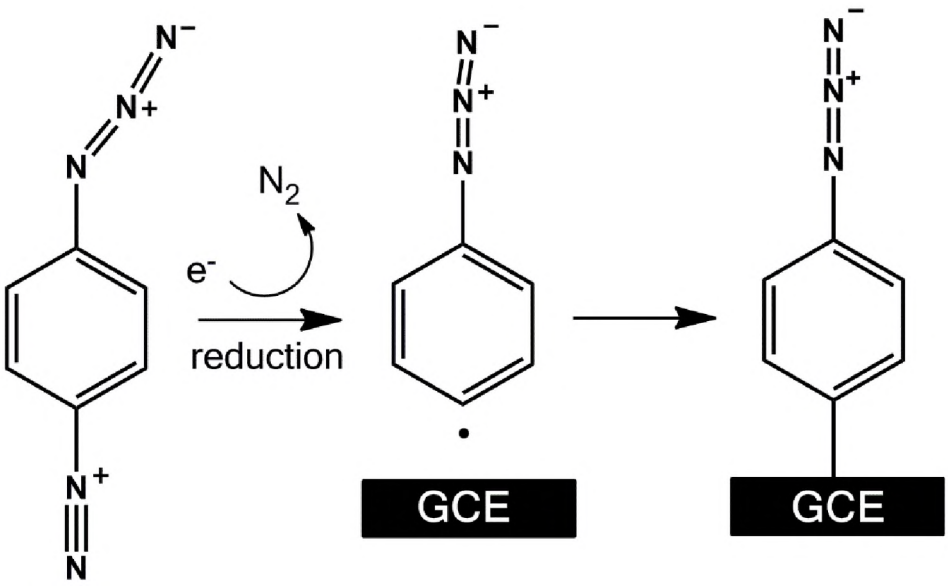

Scheme 1.2. Schematic diagram of how the electrografting reaction takes place with an azido diazonium salt grafted onto a GCE.

Scheme 1.2 is only a diagrammatic representation of the electrografting process, as monolayer formation can only be achieved by using very bulky groups in place of the azide, or by employing a radical scavenger to capture the highly reactive radical generated [25]. Due

to the highly reactive nature of the generated radical, a multi-layer is often formed [26]. This method has been used to attach an array of diazonium salts to the surface of electrodes; in order for them to be removed, the electrode surface has to be cleaned via mechanical abrasion, which is another way of confirming that it is indeed a covalent bond that forms between the surface and the diazonium salt [22,27–30]. The thickness or density of the layer formed can be controlled by varying certain parameters of the process, such as the scan rate or the concentration of the diazonium salt [22,31]. The thickness of the layer can also be controlled by adjusting the number of scans: more scans for a thicker layer and fewer scans for a thinner layer. Depending on the diazonium salt used for grafting, the electrode can be passivated by the process, especially if the layer is dense. This blocking effect can be used as a cross check to see if there are any pin hole defects in the surface [23].

This work focused on the grafting of 4-azidoaniline onto glassy carbon electrodes (GCE) and plates (GCP). This azido diazonium salt was selected as it afforded two benefits to the work: (i) the kinetics of adsorption are slower than other diazonium salts [27] and (ii) it allows for the use of the well-known Sharpless *et al.* copper(I) catalysed azide-alkyne 1,3-dipolar cycloaddition reaction, a reaction in the popular branch of "click chemistry" [27,32]. In this work, it is referred to the more commonly known "click" reaction. Table 1.1 [15,33–52] shows a selection of Pcs that have been synthesised with terminal alkyne groups as peripheral substituents and Pcs that have been used in click chemistry, together with their applications.

Table 1.1. Pc complexes and derivatives that have terminal alkyne substituents and/or terminal azide substituents, their substrates and applications.

Compound	Substrate	Application	Ref
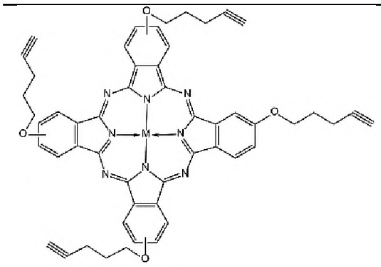	Polymer	Polymer functionalisation	[52]
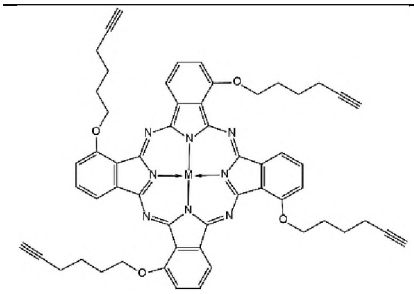	Glucose and gluco-pyranosyl M = 2H, Co and Zn	Improved water solubility	[33]
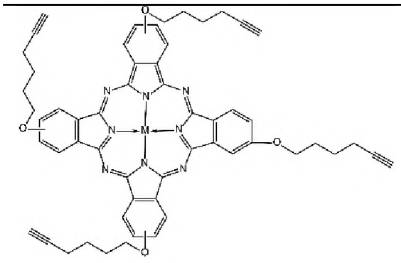	GCE – employed in this work with Mn, Co and Ni.	Electrochemical investigation	[35]
	Nanoporous gold M = Zn	Electrochemistry and photocatalysis	[36]
	GCE M= Fe	Electrocatalysis	[15]
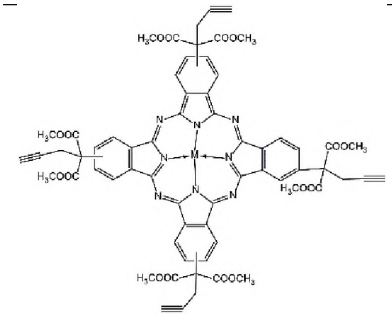	Azidomethyl phenyl sulfide	Improvement of synthetic routes	[38]

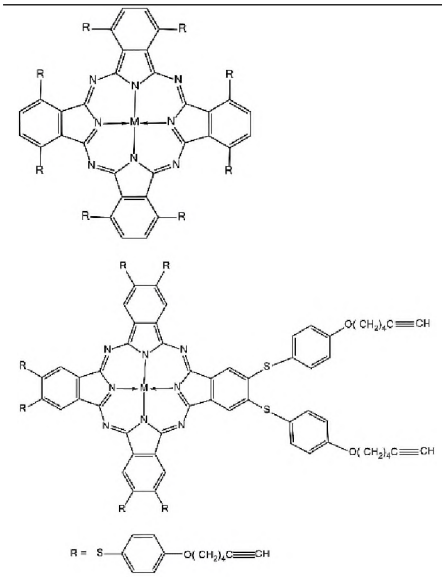	Triethylene glycol	PDT [39]
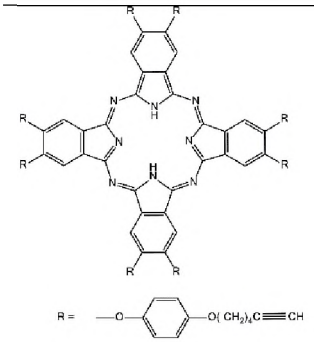	Cinnamate residues	Solvent resistant nanostructures [40]
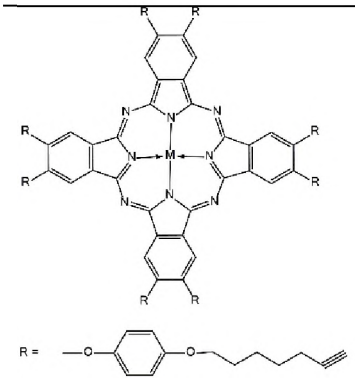	Monomethyl ether polyethylene glycol (mPEG)	Water solubility and thermal tunability [41]
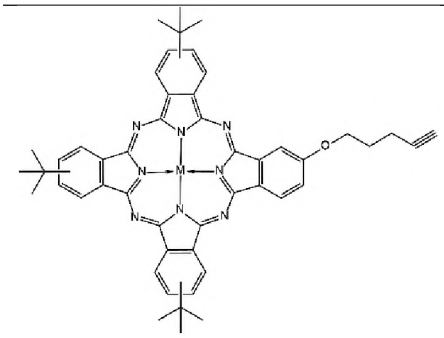	Poly(tert-butyl acrylate) (PtBA), and polystyrene (PS)	Electrochemical investigation [42]

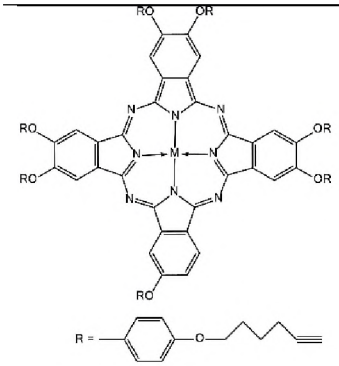	Hydrophobic, photo-crosslinkable, or electroactive azides	Preparation of multifunctional Pc derivatives	[43]
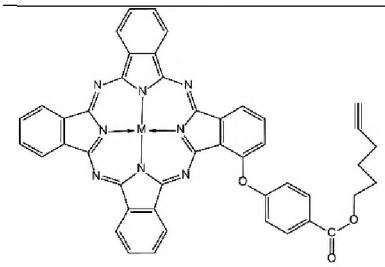	Silica nanoparticles	Photophysical stidies	[44]
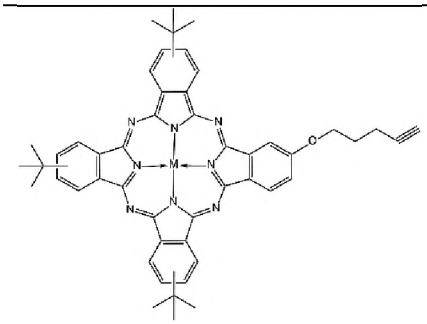	PEG	PDT	[34]
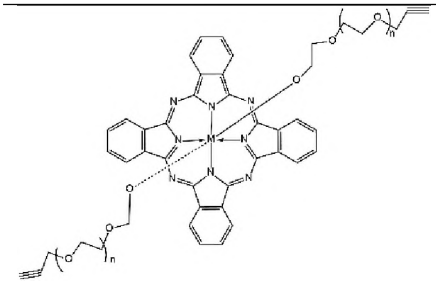	-	PDT	[45]
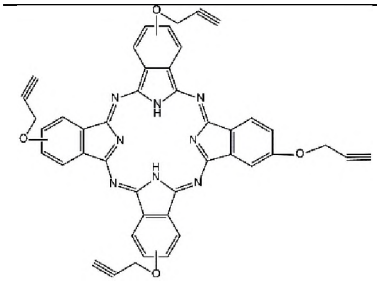	Bioconjugates M = 2H	PDT	[37]
	Oligoethylene glycol M = Zn	Improved solubility	[46]

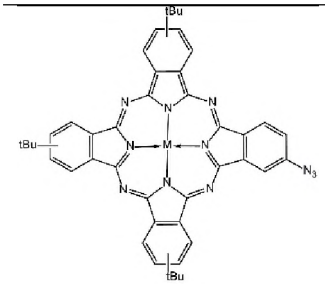	SWCNT	Spectral and electrochemical investigation [47]
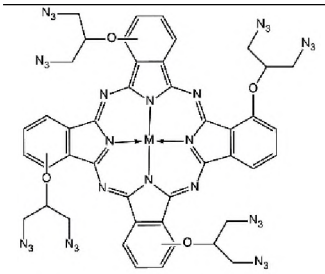	-	Photophysical applications [48]
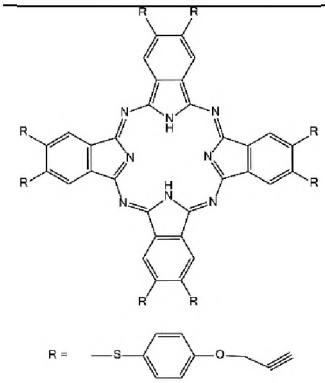	Functional group moieties	Functional group modification [49]
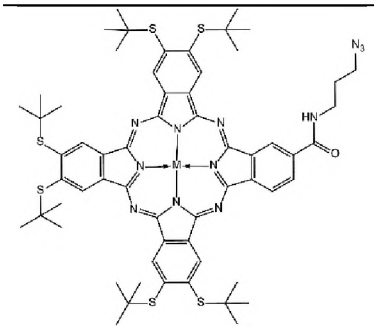 and various isomers	-	PDT [50]
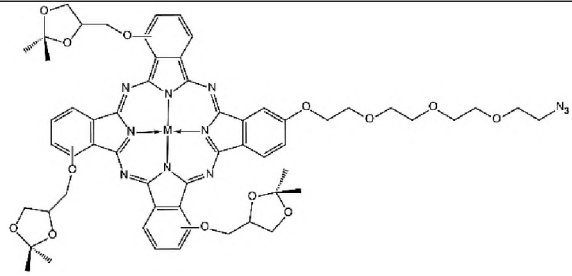	Carbohydrate units	Active targeting photosensitiser [51]

GCE = glassy carbon electrode; PDT = phtotodynamic therapy; SWCNT = single walled carbon nano tubes; PEG = polyethylene glycol;

The synthesis of terminal alkyne Pcs and azide-terminated Pcs has been done quite extensively but many of the reported cases do not involve electrochemistry. Evrard *et al.* [27] have specifically used the azide diazonium salt to electrograft to a carbon surface but with molecules such as ferrocene and biotin. From Table 1.1, Quinton *et al.* [35], Wichmann *et al.* [36], Sen *et al.* [42], Chen *et al.* [43] and Ho *et al.* [47] used their Pcs for electrochemical related work but none of them used electrografting with an azide terminated diazonium salt and carbon substrate. Nxele *et al.* [15] have carried out the same experiments presented in this work albeit with the use of iron as the central metal of the Pc. This work reports a systematic investigation of three electrochemically active metals: manganese; cobalt and nickel. The effectiveness of these three Pcs in the catalysis of hydrazine is reported for the first time. Click chemistry is discussed in more detail in Section 1.2.2.

Glassy carbon electrodes (GCEs) are a popular choice of substrate for grafting due to their inertness, ability to withstand a wide potential range, durability, and good electrochemical properties and performance [53]. These electrodes need pre-treatment to function best. Pre-treatment typically consists of mechanical cleaning by polishing the surface on a microfiber pad in an alumina slurry and sometimes diamond paste. The pre-treatment is used to improve the electron-transfer capabilities of the electrodes and ensure the electrode produces consistent results [53,54]. Carbon electrodes can be quite susceptible to poisoning or passivation, as the surface can readily form bonds to hydroxyl, hydrogen, carboxyl and quinone groups [54,55]. The cause for this bond formation can be attributed to carbon's high surface reactivity, a characteristic that also allows for easy electrode modification [54]. Due to this ease of modification, the electrodes can be modified to improve their detection limits and efficiency [56].

The grafting method employed in this work is based on that reported by Baranton *et al.* [57], who showed the direct electrochemical patterning of a diazonium salt via a one pot sequential reaction for local electrogeneration of the diazonium salt, followed by its electrografting onto the substrate [57]. This method does avoid, but not always, the spontaneous adsorption of the diazonium species onto the electrode surface, requiring very careful control of the *in situ* preparation of the salt before the grafting procedure is carried out. As shown by Cougnon *et al.* [58], the concentrations of compounds involved and electrochemical parameters can affect the formation of the grafted layer significantly [58]. The efficiency of the method

depends on the kinetics of the diazotisation reaction and the electroreduction of the diazonium salt.

1.2.2 Click chemistry

The usefulness of the electrografting can be further increased by combing the technique with click chemistry. The term "click" reaction, coined by Sharpless, was first used in 2001 and is based on an array of reactions that have to adhere to a series of criteria [59]. In order for a reaction to be considered a "click" reaction, it should have a high yield, inoffensive by-products which can be easily removed, products that are isolable via elementary methods, and simple, stable reaction conditions [59]. The reaction used in this work, one which has acquired significant interest, is the Huisgen 1, 3-dipolar cycloaddition of azides and alkynes forming a triazole via a concerted reaction mechanism, affording very high reliability and selectivity [59,60]. This reaction has been the basis for the synthesis of various organic- and bio-molecules, as well as the formation of conjugates. Additionally, it has been used in the linking of compounds to substrates such as gold, silica and glassy carbon [27,38,40,43,44,49,61–69]. The general scheme for the click chemistry reaction used in this work is shown in Scheme 1.3, where azido diazonium salt is grafted onto the GCE. Scheme 1.4 shows the attachment of an alkyne Pc to a grafted electrode, which is also to be employed in this work [15].

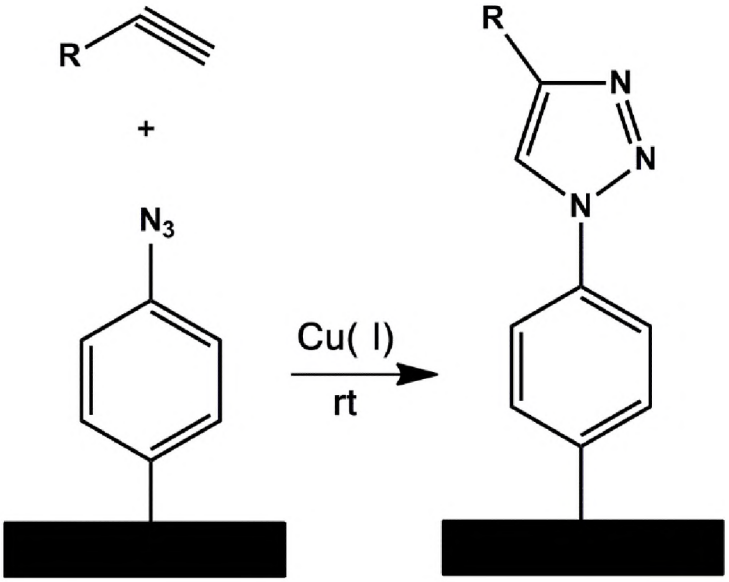

Scheme 1.3. A schematic diagram of the Huisgen 1, 3-dipolar cycloaddition "click" reaction of a substituted alkyne with an azidodiazonium grafted layer on a substrate. R = generic substituent.

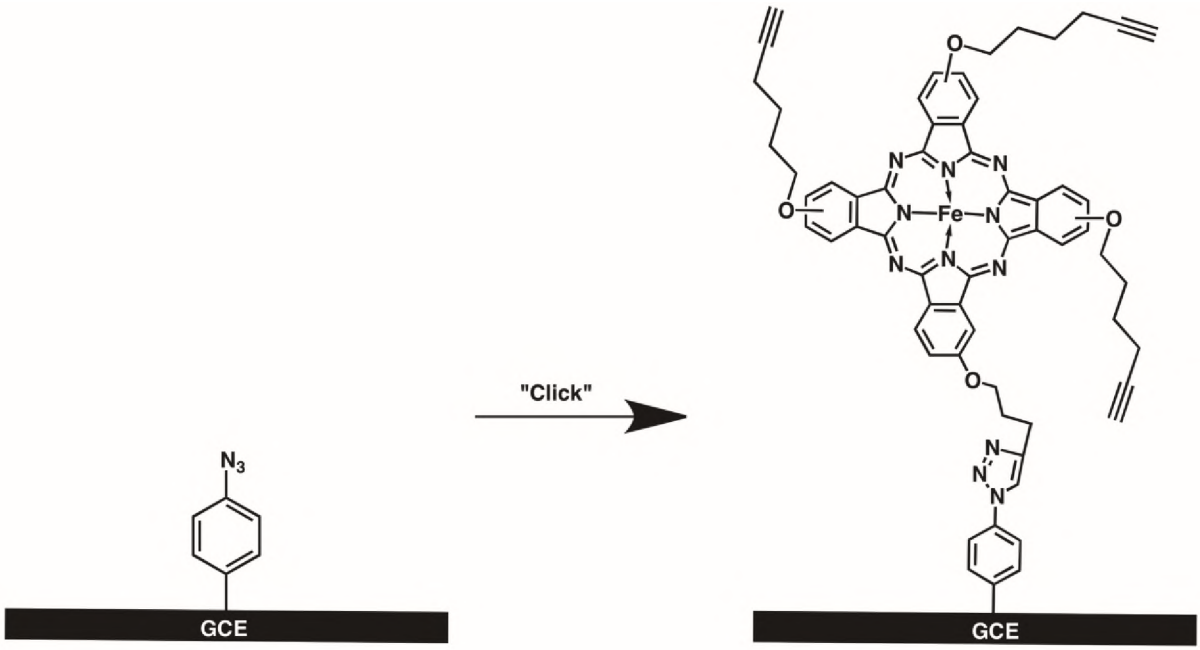

Scheme 1.4. A schematic diagram showing the covalent attachment of a Pc to the GCE via click chemistry [15].

The use of click chemistry to attach application-specific molecules and structures to substrates is growing and increasing in complexity. To the best of our knowledge, this is first the time that an investigation of manganese, cobalt and nickel's effect in the Pc ligand that has covalently bonded to the GCE via click chemistry for electrocatalysis of hydrazine has been presented.

1.2.3 Adsorption (drop dry)

This section is covered briefly as it is not used extensively in this work. This method is not a covalent form of modification. It makes use of intermolecular forces such as electrostatic attraction and the popular π-π stacking interactions to bind species to the surface in a thin layer [70]. Pcs are typically very effective in this method as they are electron rich and possess an electron cloud afforded by their extended π-system, which allows effective binding through the π-π interactions.

Adsorption has been used to modify a GCE in this work with a NiPc derivative for comparison with its clicked counterpart, in order to demonstrate a change in the surface electrochemistry that is normally observed for nickel complexes. The topic has been covered here for completeness.

1.3 Surface characterisation methods

It is of paramount importance to prove that the discussed modifications have actually taken place, and that they exist on the surfaces as imagined by theoretical speculation. Surface characterisation techniques are used to confirm successful modification. These techniques range from scanning tunnelling microscopy to X-ray photoelectron microscopy (XPS), and include electrochemical methods. Scanning electrochemical microscopy (SECM) is an exciting technique for this type of characterisation and is used extensively in this work in conjunction with XPS. These have been coupled with electrochemical techniques to elucidate how well the intended electrode modification has been carried out. With these techniques, information concerning the properties of the layers formed, the integrity of the modification, and the effectiveness of the modification can be determined. These techniques also form a significant part of the explanation as to how these modifications affect the electrocatalytic properties of the surface. These non-electrochemical techniques are often difficult to use with electrodes, as the electrodes cannot be easily placed in a sample holder, and the sensitivity required to produce useful information is very high, as the layers under consideration are very thin. To counteract these practical issues, glassy carbon plates may be employed, as they can be modified in exactly the same ways as a GCE.

Cyclic voltammetry (CV) [71], electrochemical impedance spectroscopy (EIS) [72,73] and X-ray photoelectron spectroscopy (XPS) [74–78] are among the common methods used for electrode modification characterisation and will not be discussed in detail. SECM will be briefly discussed below as it is a less common method.

SECM is a very versatile technique that has been used in many fields such as lithography, high-resolution imaging, investigation of structures and processes on the nanoscale, and alternative energy applications such as fuel cells [79]. One of the most incredible uses of the technique is the creation of images of the surface, comparable to that produced by atomic force microscopy (AFM), but generated based on the conductivity of the surface under analysis [79]. Surface topography can be observed as well as electrochemical activity [79–81]. In this work, the feedback mode of SECM was used to monitor the surface characteristics of the electrode after each step of modification.

An ultramicroelectrode (UME) is used as the electrochemical probe in SECM, together with counter and reference electrodes. The tip current is monitored and can be affected by the redox probe used as the electroactive species in solution. The conductivity of the substrate being analysed also influences the tip current and this, together with the distance of the tip to the substrate, enables analysis of the surface's electrochemical, topographic and conductive properties [81]. There are two stages at which the tip current is monitored (Fig. 1.3). To begin with, the tip current is measured while in the bulk solution and not close to the substrate surface, where a potential is applied to reduce or oxidise the species in solution. A steady current is observed, which is dependent on the concentration and diffusion coefficient of the electroactive species as well as the radius of the UME [82] Fig. 1.3 (A). The next stage at which the tip current is measured is when it is positioned near the substrate surface. From here, the nature of the surface dictates the observations made. In the case of a conducting surface, the opposite is observed whereby the diffusion of the electroactive material is enhanced and hence, an increase in current is observed Fig. 1.3 (B). When the substrate is of an insulating nature, diffusion at the tip is blocked and results in a reduction of the current measured Fig. 1.3. (C) [81,83].

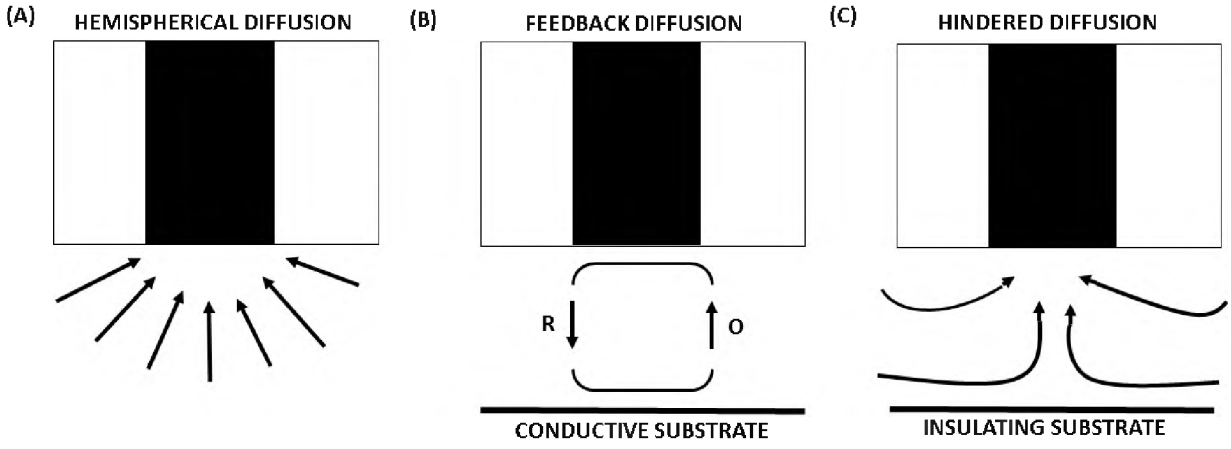

Figure 1.3. Basic principles of scanning electrochemical microscopy (SECM): (A) far from the substrate, diffusion leads to a steady-state current. (B) Near a conductive substrate, feedback diffusion leads to increased current. (C) Near an insulating substrate, hindered diffusion leads to decreased current [80].

The SECM techniques that are of interest in this work are the approach curves and area scans. The approach curve is generated by slowly lowering the tip towards to the surface from a bulk solution position that is far from the surface. This technique produces a curve that shows

conductivity changes with respect to distance from the surface, which is useful for extracting kinetic information [80]. The area scan technique is typically done when the tip is near the surface and thus directly affected by the conducting or insulating nature of the surface. From this point, the tip is moved across the surface in a systematic fashion, all the while measuring the current, producing a three dimensional image of the surface based on its conductivity [79,80]. Fig. 1.4(a) shows two approach curves illustrating the difference between conductive and insulating surfaces. As the UME is moved closer to the surface (positioned at zero), an insulator, which hinders electron movement, will result in a reduction of current, and hence a downward curve. Conversely, a conducting surface generates an upward curve, as it enhances electron movement. Fig. 1.4(b) shows an area scan of an electrode that has had half of its surface modified with an insulating layer, while Fig. 1.4(c) provides a top view of the same data as in Fig. 1.4(b), showing a patch plot of the conductivity as spread over a small area of the electrode surface [84]. While SECM is capable of performing a whole range of different techniques, the approach scan and area scan are the most relevant techniques in the context of this work.

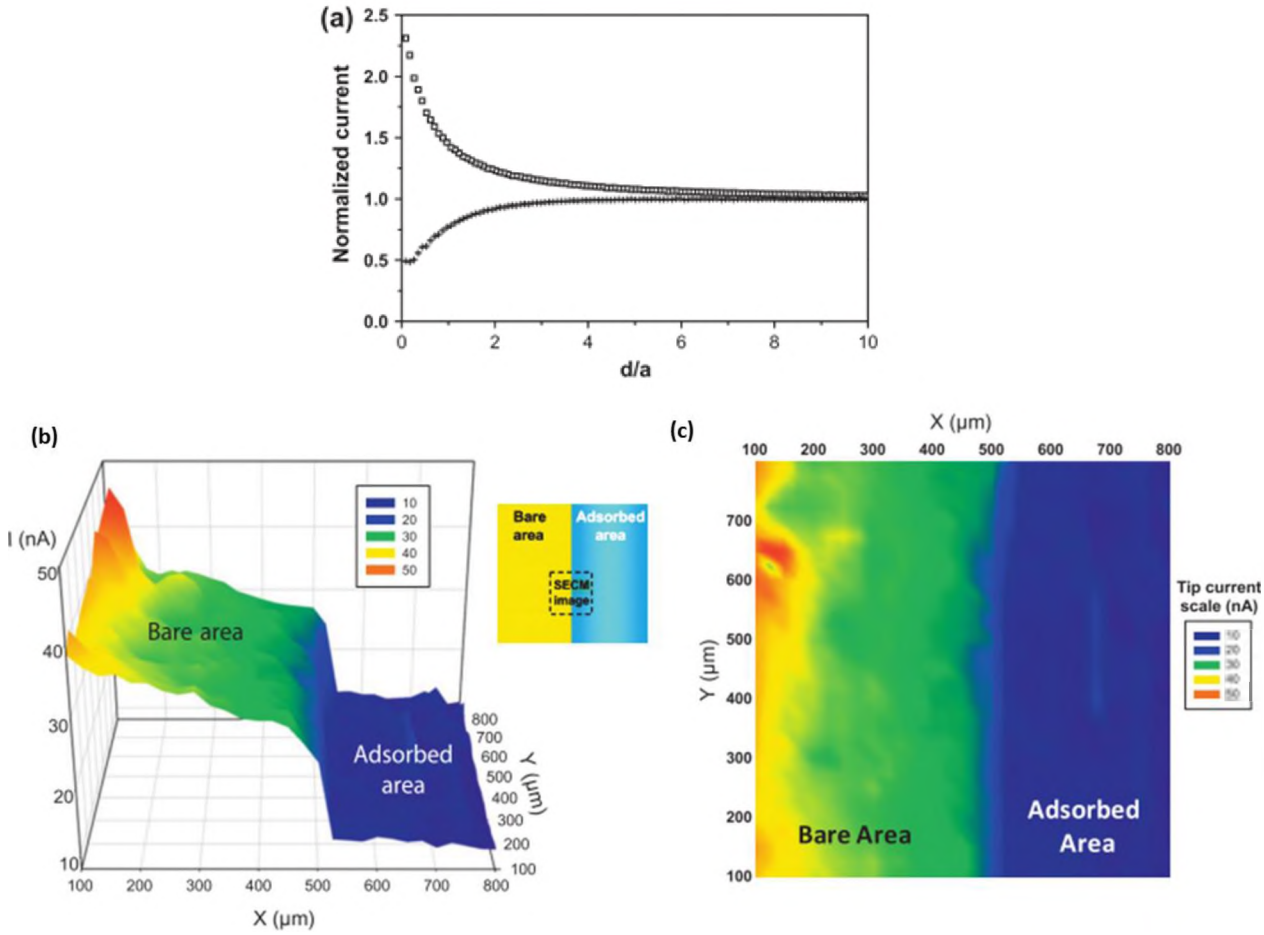

Figure 1.4. SECM examples of the approach curve technique (a), where both a conducting and insulating surface have been analysed. An area scan example of a surface that is part conducting and part insulating due to a modification made to it. Part (b) shows a 3D side view of the data and part (c) shows a top view, in the form a patch plot [84].

1.4 Electroanalytical techniques and analytes employed in this work

Accurate detection of analytes is especially important when the compounds of interest pose health risks or have the capacity to negatively impact the environment. Often, these toxic target analytes are present in extremely low concentrations, thus making their detection difficult but imperative, especially as small variations in their concentration can induce more widespread effects. The use of electrocatalysis, the acceleration of an electrochemical reaction in the presence of a catalyst, to detect target analytes, has shown to hold many benefits [54]. When cyclic voltammetry (CV) is used to perform electrocatalysis, there are two distinctive properties of the resultant CV that indicate an improvement in electrocatalytic behaviour: firstly, a movement in the potential toward the zero mark and, secondly, an increase in current as a result of the catalysis, which would also mean an increase in sensitivity [85]. An example of how a modified surface can induce higher currents and shift the electrocatalysis peak toward the zero mark is shown in Fig. 1.5 [86].

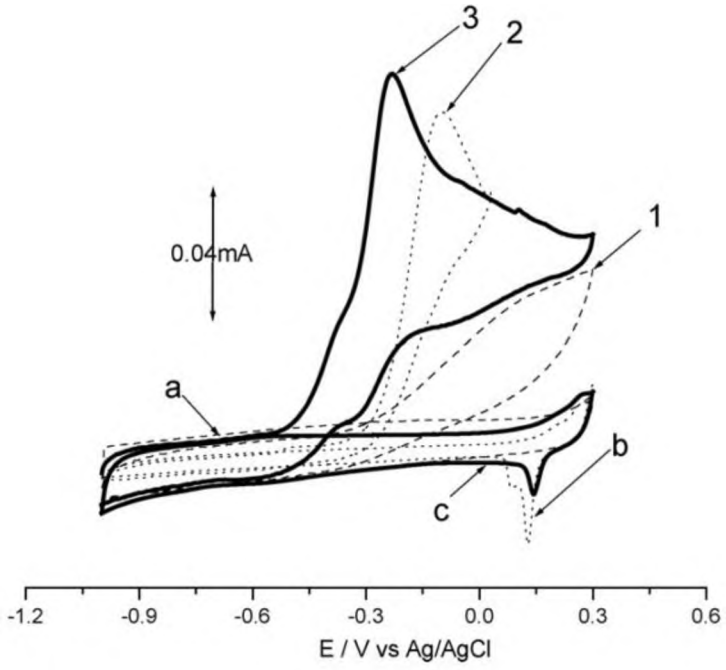

Figure 1.5. CV showing three curves: 1-3. Curve 1 shows an electrode modified with only SWCNT. Curve 2 shows an electrode modified with a CoPc only. Curve 3 shows an electrode where the SWCNT and CoPc have been combined to achieve the best result. Curves a, b and c represent each of the surfaces mentioned above but run in a buffer solution without the target analyte [86]. SWCNT = Single walled carbon nanotube.

Another electrochemical technique that is used in analyte detection is chronoamperometry. Chronoamperometry is more sensitive and systematic than CV and can therefore be used to determine the limit of detection (LoD) of an electrode for a particular analyte, as well as the sensitivity of the electrode. This technique is performed by submerging the electrode in a solution containing an electrolyte and the target analyte. A certain potential is then applied to the electrode. Typically, this potential is found from the peak in the CV of the electrode and target analyte. This potential is applied for a select period of time. The peak found from CV and subsequently used in chronoamperometry, is the point at which the target analyte is reduced or oxidised. From the chronoamperometric data, a plot of current versus concentration is used to obtain the LoD and the sensitivity.

Metallated Pcs are among the many materials that have been shown to have electrocatalytic activity towards certain target analytes and this affords them the ability to be used in the field of electroanalytical sensing [1]. Electroanalytical sensing has been applied as an accurate detection tool for medical, agricultural and safety purposes. Therefore, hydrazine has been chosen as an analyte of significance due to its toxicity and potential carcinogenicity and mutagenicity [87,88]. Hence, all electrodes in this work were used to test for hydrazine in solution. Hydrazine is an oxidising agent used in many areas but is also very toxic. It can be easily absorbed via inhalation, ingestion and through the skin [89]. Low doses of hydrazine can act as a central nervous system depressant and high doses cause convulsions [89]. . Hydrazine is used in water treatment; as a pesticide in agriculture; and in the formation of plastics, and has been reported to hold potential as an alternative fuel in fuel cells [89]. Metallated Pcs have been reported many times for their electrocatalytic activity towards hydrazine, making this analyte particularly useful in testing the modified surfaces [15,90].

1.5 Aims

The aims of this work were to explore the use of click chemistry to covalently attach metallated Pcs to the surface of glassy carbon electrodes and then systematically compare the effect of the metal centre on the effectiveness of the sensors produced by the surface modification.

1. Synthesise and characterise the new Pc derivatives containing Co and Ni as their central metals.
2. Study the grafting of 4-azidoaniline hydrochloride and click chemistry with peripherally substituted metallated Pcs with terminal alkyne groups.
3. Use SECM, XPS, EIS and CV as surface characterisation techniques to elucidate the success of the modification approach and examine the varied properties of the electrode surface at each stage of modification.
4. Compare manganese, cobalt and nickel as central metals for MPcs in their effectiveness for the catalytic oxidation of hydrazine.

CHAPTER 2

EXPERIMENTAL

2.1 Materials

Pure water was obtained from Milli-Q Water Systems (Millipore Corp. Bedford, MA, USA). Alumina (~0.05, 0.3, 1, 10 µm), 4-azidoaniline hydrochloride, 1,8-diazabicyclo[5.4.0]undec-7-ene (DBU), dimethylformide (DMF), dimethylsulfoxide (DMSO), copper(I)complex ($Cu(PPh_3)_3Br$), tetrabutyl ammonium tetrafluoroborate ($TBABF_4$), urea, trimethylamine and hydrazine monohydrate were purchased from Sigma Aldrich and used as they were received. Acetonitrile (ACN) was obtained from Minima. Iron ferricyanide and iron ferrocyanide were obtained from Unilab and used as received. Dichloromethane (DCM) was obtained from B&M Scientific. 4-Azidobenzenediazonium tetrafluoroborate salt was synthesized from 4-azidoaniline hydrochloride *in situ* as reported in literature [27]. Nickel chloride and quinoline were obtained from Merck. Cobalt chloride was obtained from Saarchem. The syntheses of 4-(hex-5-yn-oxy) phthalonitrile (**1**) and tetrakis(5-hexyn-oxy) manganese(II) phthalocyanine (**2**) have been reported [35].

2.2 Equipment

An Autolab PGSTAT30 electrochemical workstation (equipped with GPES software version 4.9) was used for cyclic voltammetry (CV), chronoamperometry and electrochemical impedance spectroscopy (EIS). A three electrode electrochemical cell comprising of a glassy carbon electrode (GCE) (geometric area = 0.071 cm^2) as the working electrode, Ag|AgCl (3 M KCl) as reference electrode, and a platinum wire as the counter electrode was employed. The GCE surfaces were polished on a Buehler-felt pad using alumina (10; 1; 0.3; 0.05 µm). The glassy carbon plate (GCP) (used for SECM and XPS) was power cleaned using 3 µm diamond paste, followed by 0.25 µm diamond paste and then polished on a Buehler-felt pad using alumina (10; 1; 0.3; 0.05 µm). For all electrodes, following the polishing step, sonication was carried out for 5 min in Millipore water to remove any impurities. The surfaces were then rinsed with Millipore water and dried in air.

Scanning electrochemical microscopy (SECM) experiments were conducted using Uniscan equipment, model 370 and a 25 µm Pt ultra-microelectrode (UME) as the tip. Approach curve analysis and constant height imaging were employed. The 25 µm Pt micro-electrode was used

together with a Pt counter electrode and Ag|AgCl wire as the pseudo-reference electrode. Changes were monitored in the steady state current of $K_3[Fe(CN)_6]$ oxidation at variable voltages vs. Ag|AgCl.

X-ray photoelectron spectroscopy (XPS) was done using a Kratos Axis Ultra DLD, with the Al (monochromatic) anode, equipped with a charge neutraliser. For wide XPS scans, the following parameters were used: emission 10 mA, anode (HT): 15 kV, operating pressure below 5×10^{-9} Torr, hybrid lens, and resolution to acquire scans was at 160 eV pass energy in slot mode. The centre used for the scans was at 520 eV and the width at 1205 eV, with steps at 1 eV and dwell time at 100 ms. For the high resolution scans, the resolution was changed to 80 eV pass energy in slot mode. Centre was at 402 eV and width at 12 eV for N(1s), with step size at 0.05 eV and dwell time at 500 ms. Glassy carbon plates (1 cm x 1 cm and 2 mm thick) were obtained from Goodfellow, UK and employed for SECM and XPS studies.

Infrared (IR) spectra were recorded on a Bruker Alpha IR (100 FT-IR) spectrophotometer. Elemental analyses were done using a Vario-Elementar Microcube ELIII, while mass spectra data were collected on a Bruker AutoFLEX III Smart-beam TOF/TOF mass spectrometer using α-cyano-4-hydrocinnamic acid as the matrix in the positive ion mode. Ground state electronic absorption spectra were recorded on a Shimadzu UV-2550 spectrophotometer.

2.3 Synthesis

2.3.1 Tetrakis(5-hexyn-oxy) cobalt(II) phthalocyanine (3), Scheme 3.1

The synthesis of tetrahexynl coablt phthalocyanine (**3**) was carried out using procedure for tetrakis(5- hexyn-oxy) MnPc [35] by dissolving 4-(hex-5-yn-oxy) phthalonitrile (**1**) (0.1 g, 0.450 mmol) and $CoCl_2$ (0.026 g, 0.2 mmol) in 1-pentanol (3 mL). DBU (35 µL) was added and the mixture stirred for 12 h under argon atmosphere while refluxing at 140 °C. The blue mixture was left to cool and precipitated out using a methanol-water mixture and collected by centrifugation. The collected precipitate was washed several times with 1 M HCl, methanol and finally millipore water and collected again by centrifugation. IR: KBr ν (cm^{-1}): 742, 821, 964, 1093(Pc ring), 1229, 1276, 1333, 1386, 1388 (C-O-C), 2112 (C≡C), 3307 (C-H, alkyne). UV-vis (DMF): λ_{max}/nm (log ε): 337 (4.20), 613 (3.96), 676 (4.46). MALDI-TOF-MS (m/z): amu found

= 955 amu; calcd. [M]+ = 955.31 amu. Anal. calcd. for $C_{56}H_{48}CoN_8O_4$: C 70.36, H 5.06, N 11.72%. Found: C 70.08, H 5.42; N 9.60 %.

2.3.2 Tetrakis(5-hexyn-oxy) nickel(II) phthalocyanine (4), Scheme 3.2

The sysnthesis of tetrahexynl nickel phthalocyanine (**4**) was carried out using a similar procedure to Gurek et al. [91] by dissolving 4-(hex-5-yn-oxy) phthalonititrile (**1**) (0.1 g, 0.450 mmol), urea (1.5 g, 25 mmol) and $NiCl_2$ anhydrous (0.1020 g, 0.79 mmol) in quinoline (8 ml). The mixture was heated at 200 °C while stirring and under argon atmosphere for 5 h. The dark green mixture was left to cool before being treated with cooled ethanol. The precipitate was collected and subsequently boiled in water. Finally the precipitate was purified via column chromatography on neutral silica gel with chloroform as the eluent. The deep cyan NiPc was dried and collected as a fine powder. IR: KBr ν (cm^{-1}): 738, 809, 964, 1054(Pc ring), 1229, 1254, 1337, 1388 (C-O-C), 1390, 2110 (C≡C), 3279 (C-H, alkyne). UV-vis (DMF): λ_{max}/nm (log ε): 331 (4.20), 611 (4.21), 674 (4.43). MALDI-TOF-MS (m/z): amu found = 958.33 amu; calcd. [M]+ =958.35 amu. Anal. calcd. for $C_{56}H_{52}NiN_8O_4$: C 70.08, H 5.46, N 11.68%. Found: C 69.35, H 7.41, N 9.89 %.

2.4 Electrode Modification

2.4.1 Grafting, Scheme 4.1

The grafting procedure was carried out by using an *in situ* diazotised 4-azidoaniline hydrochloride salt. Briefly, 1 mM of 4-azidoaniline hydrochloride was prepared in 96:4 ACN/ 1 M HCl with 0.1 M $TBABF_4$. The deaerated solution was cooled to 0 °C for 15 min and 3 mM of $NaNO_2$ was added. After a further 15 min period, the bare GCE surface was grafted (Scheme 4.1) by electrodeposition and scanning from +0.5 V to -1 V for 5 cycles at 50 mV/s in a solution of, now, 1 mM 4-azidobenzenediazonium tetrafluoroborate (**5**) (containing 0.1 M $TBABF_4$ in 96:4 ACN:HCl (1 M)) following reported methods [21,92]. Between each step of grafting, the electrode was rinsed thoroughly via ultrasonication for 5 min with DMF, then absolute ethanol and then milli-Q water, to give grafted-GCE.

2.4.2 Click chemistry, Scheme 4.2

Following the grafting step, the click reaction (Scheme 4.2) was performed by immersing the grafted electrode into a solution containing 0.1 µM **2** or **3** or **4** in 5mL DMF containing 2 mM $Cu(PPh_3)_3Br$ and 2 ml triethylamine. The electrode was left to 'click' with complexes **2** or **3** or **4** for 18 h, represented as **2**-clicked-GCE or **3**-clicked-GCE or **4**-clicked-GCE. The glassy carbon plate (GCP) surfaces used for SECM and XPS were grafted and 'clicked' via the same process as applied to the GCE, represented as bare-GCP, grafted-GCP and **2**-clicked-GCP or **3**-clicked-GCP or **4**-clicked-GCE.

RESULTS AND DISCUSSION

This section has been split into three chapters:

Chapter 3: Metallophthalocyanine synthesis and characterisation

Chapter 4: Electrode modification

Chapter 5: Electrocatalytic studies

PUBLICATIONS

Most of the work presented in the following chapters has been published in these articles:

1. Charles S. J. N. O'Donoghue, Gertrude Fomo & Tebello Nyokong. Electrode Modification Using Alkyne Manganese Phthalocyanine and Click Chemistry for Electrocatalysis. *Electroanalysis*, **28**, 3019–3027 (2016).

The following article has been accepted for publication:

2. Charles S. J. N. O'Donoghue, Munyaradzi Shumba & Tebello Nyokong. Electrode Modification Through Click Chemistry using Ni and Co Alkyne Phthalocyanines for Electrocatalytic Detection of Hydrazine. *Electroanalysis*, **29**, 1731–1740 (2017).

CHAPTER 3

METALLOPHTHALOCYANINE SYNTHESIS AND CHARACTERISATION

The alkyne phthalonitriles were reacted with their respective metal by refluxing in either 1-pentanol or quinoline for either 12 h or 5 h. The structures of these complexes are shown in Schemes 3.1 and 3.2.

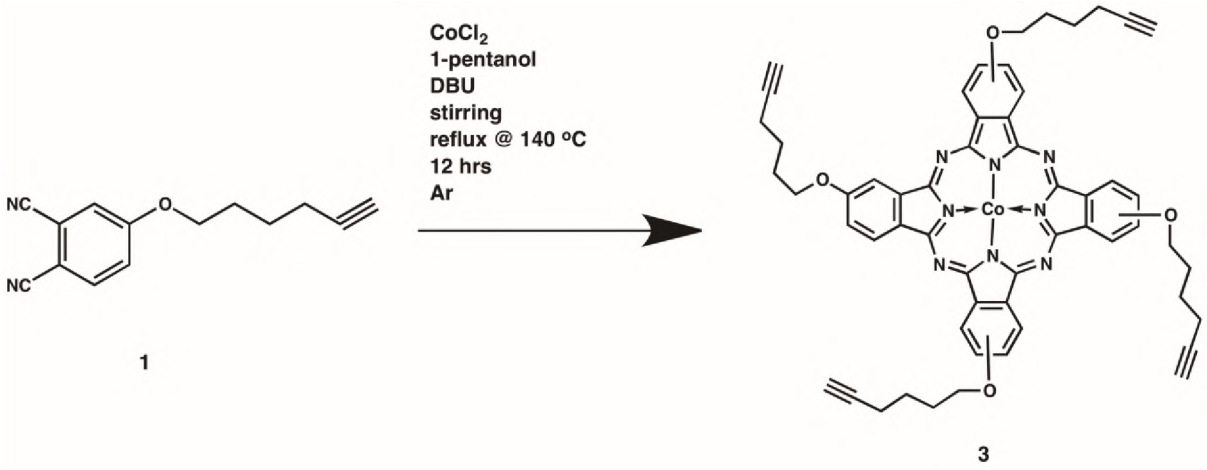

Scheme 3.1. Synthetic route for the produced tetrakis(5-hexyn-oxy) cobalt(II) phthalocyanine (**3**).

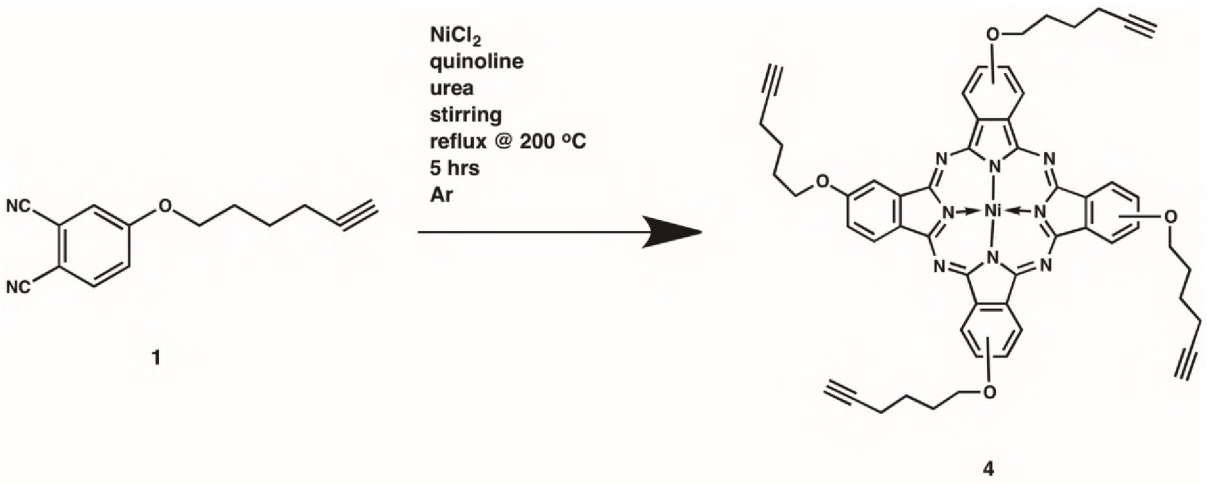

Scheme 3.2. Synthetic route for the produced tetrakis(5-hexyn-oxy) nickel(II) phthalocyanine (**4**).

A mixture of four possible structural isomers is expected for complexes **2**, **3**, and **4**. The four probable isomers can be designated by their molecular symmetry as C_{4h}, C_{2v}, C_s and D_{2h}, and they are known to occur in an expected statistical mixture of 12.5% C_{4h}, 25% C_{2v}, 50% C_s and 12.5% D_{2h} for peripherally substituted complexes [93]. The isomers are known to be difficult to separate and thus no attempt was made to separate them in this work

Apart from the mentioned aggregation complexes **3** and **4** showed good stability, especially complex **3**.

The formation of the complexes was also confirmed by the presence of the C-H stretches in the IR spectra. The C-H stretch on the terminal alkyne tends to appear as a strong, narrow band at 3307 (**3**) and 3279 (4) cm^{-1} and the triple bond is observed as a weak peak at 2112 (**3**), 2110 (**4)** cm^{-1}. A final part of the confirmation of the structure with IR was the observation of the glycosidic linkage, typically seen at approximately 960 cm^{-1}. Both complexes, **3** and **4**, exhibited this band in their IR spectra at 964 cm^{-1}.

The UV-vis spectra for **3** and **4** has been shown in Fig. 3.1 and it is clear their Q bands are very near to each other. Complex **3** has its Q band at 676 nm and complex **4** at 674 nm. The slight blue shifting in the Q bands from complexes **3** to **4** can simply be attributed to the change in the central metal from cobalt (II) to nickel (II). Complex **2** was observed to have red shifting, which is typical of Mn^{III} PC complexes [3]. In addition to spectral shifts observed as a result of the central metal, red shifting in all the complexes can also be attributed to the electron donation made into the metal centre by the electron rich terminal alkyne groups [94].
The complexes had absorption bands in the 400-380 nm range which could be attributed to charge transfer between the metal and the Pc ring [3]. Beer's law was observed for all complexes at concentrations less than 15 µM. Q band maximums are compared for these two Pcs as well as other Pcs of similar structure from literature in Table 3.1.

Table 3.1. Q band wavelength of complexes **3** and **4** in DMF, unless otherwise indicated.

Complex	**Q band wavelength (nm)**	**Reference**
2	732	[35]
3	676	This work
4	674	This work
thFePc[a]	700[b]	[15]

[a] tetrakis(5-hexyn-oxy) iron(II) phthalocyanine

[b] In DMSO

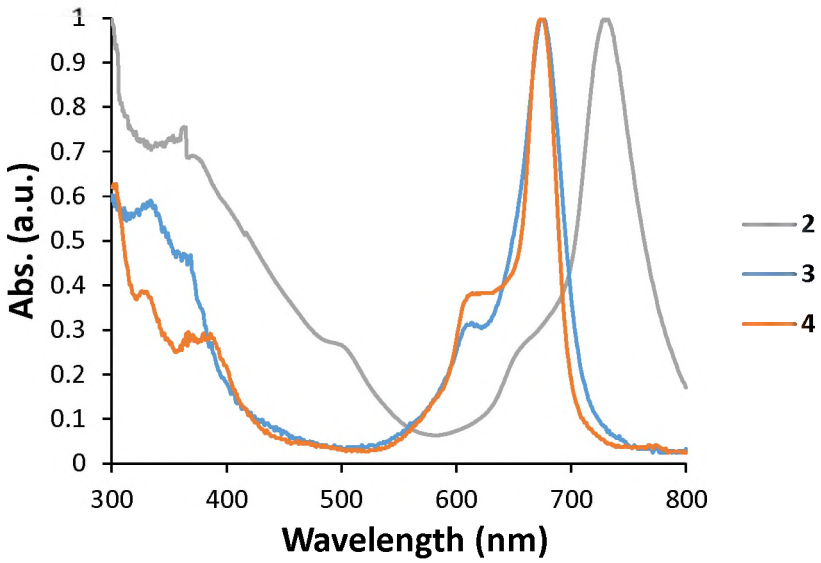

Figure 3.1. UV-visible spectrum of **2**, **3** and **4** in DMF (15 μM).

Both complexes showed good solubility in DMF. However, after being dried and kept for over a week, their solubility in DMF was not as consistent as especially the nickel tended to aggregate as shown in Fig. 3.2. The red shifting in complex **2** is typical of Mn^{III} Pc complexes [3].

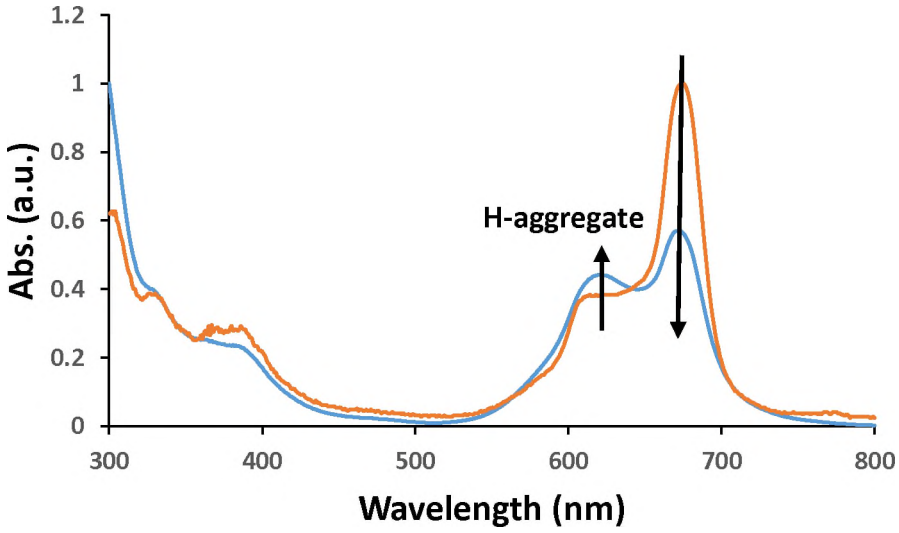

Figure 3.2. UV-visible spectrum of complex **4** in DMF before (blue) and after (orange) ultra-sonication to reduce aggregation, shown by increase of vibronic band (H) and reduction of the Q band.

Aggregation known as "H" aggregation [3] in MPc is evidenced by a split Q band – showing an increase in the high-energy band and a decrease in the low energy band. This aggregation

occurs as a result of π-π stacking of the MPcs [3]. Ni MPcs are known to aggregate and hence, this behaviour is not unexpected [95].

In conclusion, the two new MPcs, complexes **3** and **4** were successfully synthesised and characterised. Both exhibited usual IR bands and showed typical behaviour in the UV-vis spectra.

CHAPTER 4

ELECTRODE MODIFICATION

4.1 Surface modification by grafting of 4-azidobenzenediazonium (5)

In this work grafting was used in combination with click chemistry to attach a series of Pcs to the electrode surface. The approach employed in the work is of the type graft-then-click. This approach involves the introduction of azide groups onto the electrode surface through *in situ* diazotisation of 4-azidoaniline hydrochloride to form **5** and electrochemical grafting of 4-azidobenzenediazonium (**5**), followed by click chemistry with complexes **2**, **3**, and **4**. The structures of the fundamental complexes are shown in Fig. 4.1.

To begin with, the electrochemical grafting of **5** on the GCE and GCP will be discussed, followed by the subsequent reactions using click chemistry.

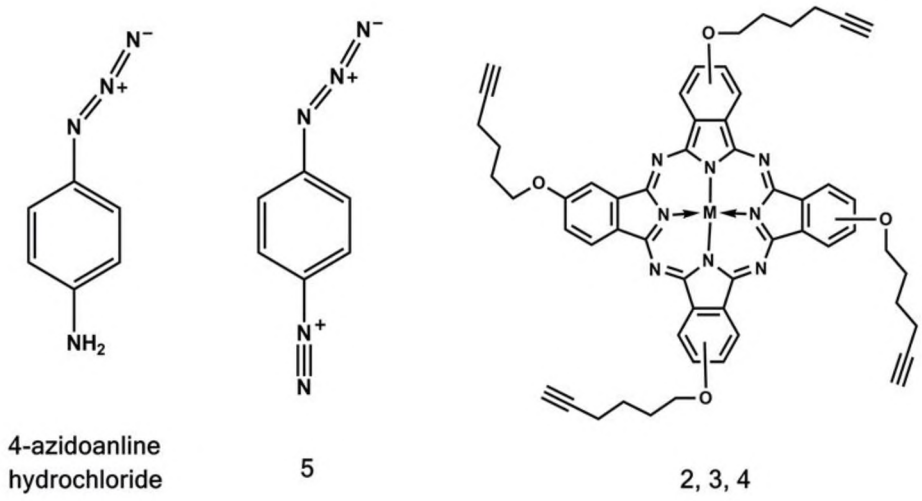

Figure 4.1. Complexes used for grafting and click chemistry

Electrochemical grafting was used to modify GCEs through *in situ* diazotisation of 4-azidoaniline to **5** and grafting. *In situ* diazotisation was done by addition of sodium nitrite in aqueous acidic media [96,97]. This approach was first shown by Delamar *et al.* [21] and has proven to be a gateway to many possibilities. Scheme 4.1 shows the grafting process in a step by step manner as well as a schematic of how **5** is expected to bond to the surface of the electrode.

Fig. 4.2 shows how the grafting process can be observed through CV. In the first cycle two broad reduction peaks are seen and in subsequent scans the peaks decrease significantly until they are almost untraceable. This occurs as a result of the electrode becoming passivated by the blocking effect brought on by the bonding of the diazonium salts to the surface. The process by which this takes place has been well studied, but in brief, reductive electron

transfer to the diazonium salt takes place, which is followed by the cleavage of the dinitrogen, generating aryl radicals, which then bind to the surface of the electrode via carbon to carbon single bonding [22,27,29,57].

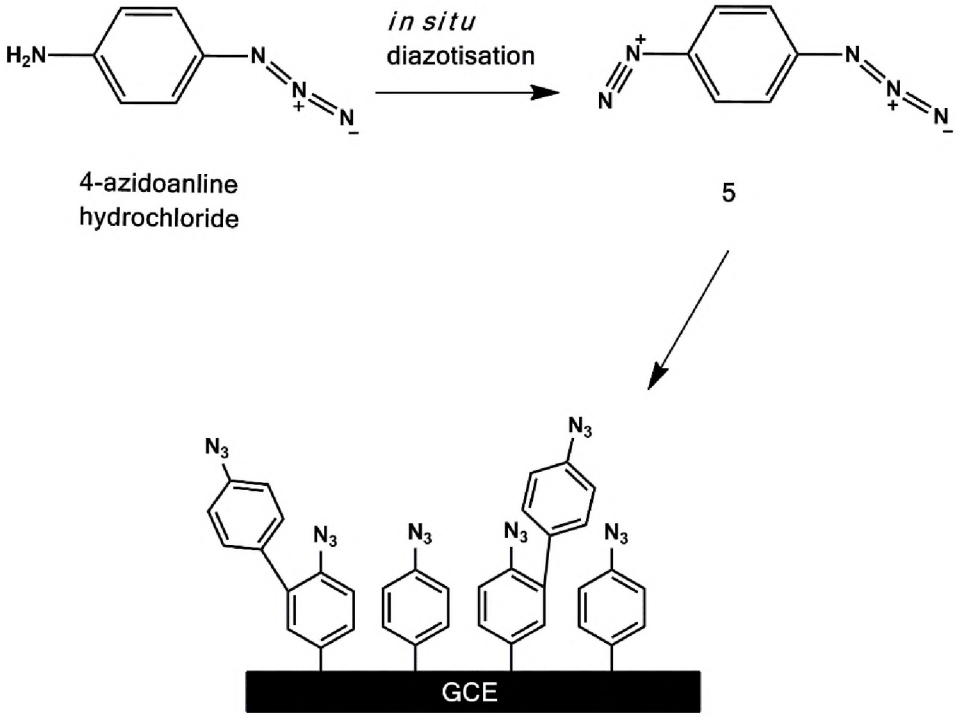

Scheme 4.1. Proposed electrochemical grafting approach employed in this work.

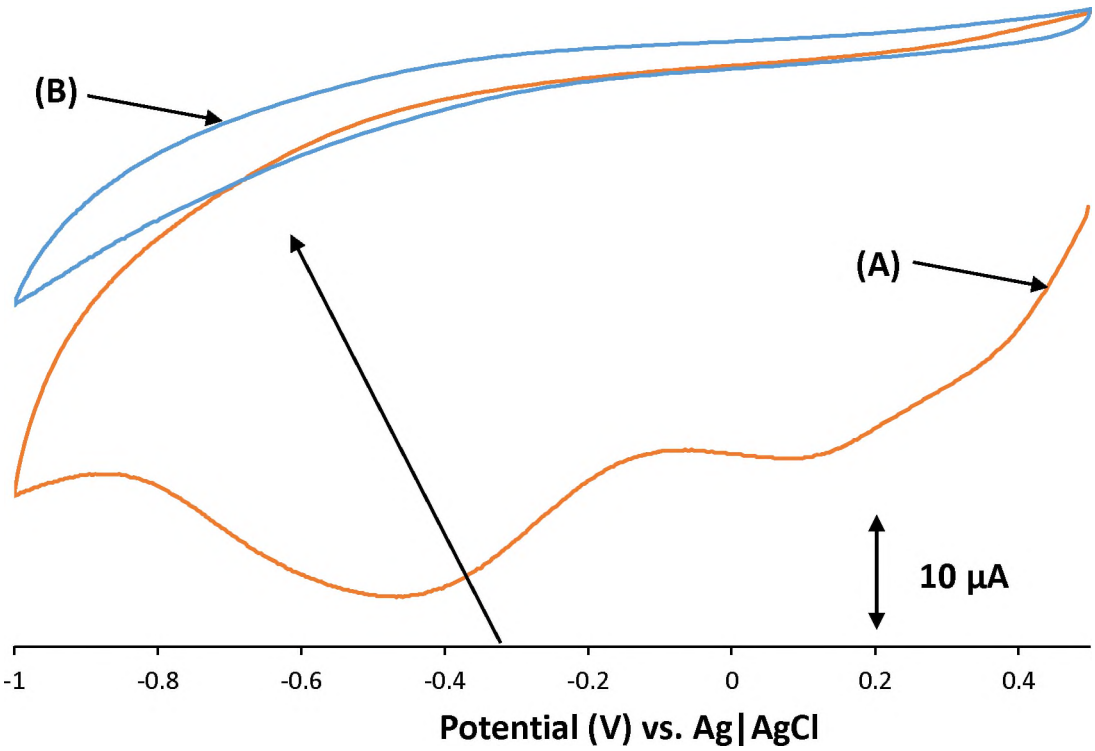

Figure 4.2. Electrochemical grafting of GCE in 1mM **5** in 0.1M $TBABF_4$ in ACN: 1 M HCl (96:4). Five cycles at 50 mV/s vs. Ag|AgCl. (A) is the first scan and (B) is the fifth scan.

There are two main peaks observed during the first at about 0.10 and -0.46 V. Similar peaks to these have been reported before by Baranton and Bélanger albeit in a more positive range with other diazonium salts for the *in situ* generated diazonium [57]. The shape of the CVs are also similar to other reported work in literature where other diazonium salts are used, but producing the large peak in the first scan and followed by a reduction in that peaks intensity in subsequent scans [27,57,92,97]. However, it is typical for there to be one reduction peak for diazonium salts, but there have been several explanations for the presence of two. It has been believed in one case to be due to the graphitic planes and edges of the carbon electrode surface [24]. The origin of the first peak has been, in some cases, classified as unknown, with the second being attributed to the reduction of the diazonium [30]. The first peak has been, in other cases, attributed to the presence of adsorbed species at the surface [98].

4.1.1 Cyclic voltammetric characterisation

To prove that the grafting was successful, the effect of the passivation, induced because of the blocking effect brought on by the grafting, was investigated by cyclic voltammetry in

$K_4[Fe(CN)_6]$ where the redox process is expected to be lost [15]. Fig. 4.3 shows the surfaces before and after grafting with **5**. A complete suppression of the redox behaviour of ferrocyanide following grafting was observed. A compact layer was formed.

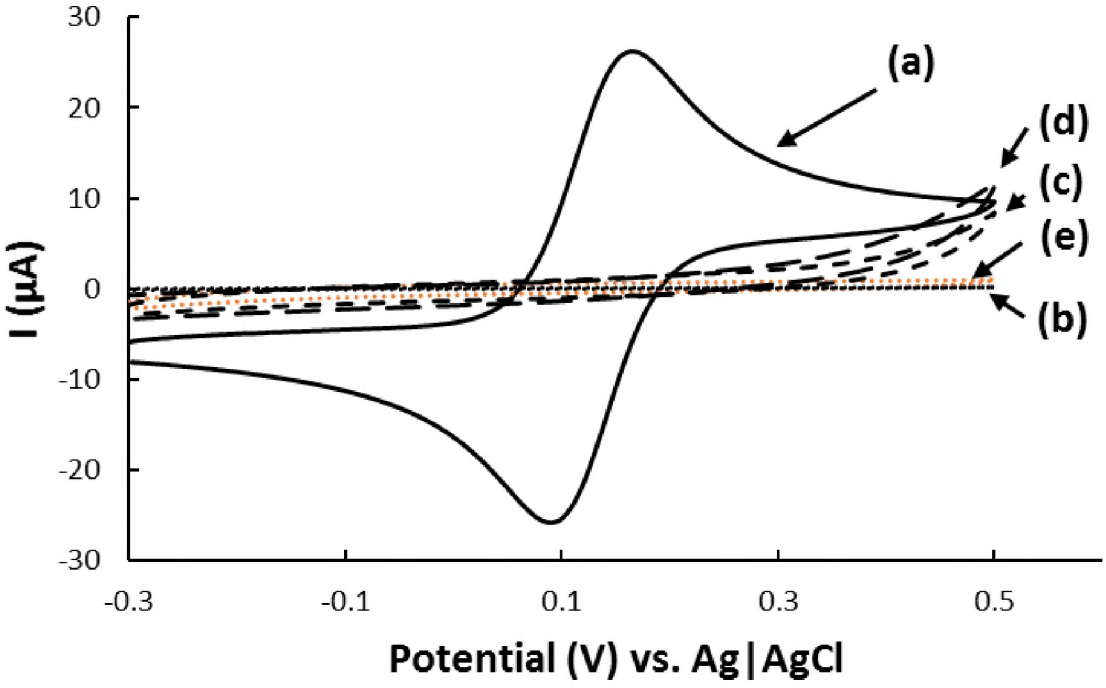

Figure 4.3. Cyclic voltammograms of the three surfaces after electrografting and click chemistry showing the retention of the blocking effect, (a) bare-GCE, (b) **2**-clicked-GCE, (c) **3**-clicked-GCE, (d) **4**-clicked-GCE and (e), also shown in orange, represents the grafted-GCE. CVs in 1mM $K_4[Fe(CN)_6]$ in 0.1 M KCl.

4.1.2 Scanning electrochemical microscopy (SECM)

SECM was used to confirm the blocking of the electrode, and gain insight as to the electron transfer kinetics of the surface. Glassy carbon plates (GCP) were used for SECM analysis and were grafted in the same way as the GCEs.

SECM approach curves were carried out with a constant potential applied to the platinum tip of the ultramicroelectrode (UME) to oxidise the ferrocyanide in solution. The current at the tip was monitored as the tip was lowered toward the unbiased substrate. Approach curves are plotted with the current measured (I) and distance (*d*) normalised with respect to the limiting current, I_{LIM}, and the radius of the probe (*a*) respectively. Fig. 4.4shows the SECM

approach curves to the grafted surfaces and compares the response with approach curves to the bare GCP surface and bare Teflon ®, which is worked from as a benchmark as an almost ideal insulator.

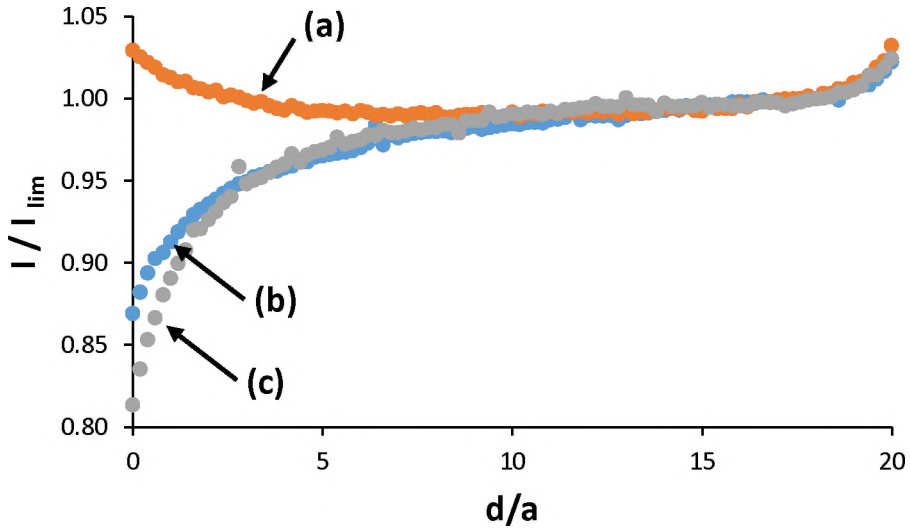

Figure 4.4. SECM approach curves using 25 µm Pt UME in 5mM $K_4[Fe(CN)_6]$ in 0.1 M KCl. Approach to (a) bare-GCE, (b) grafted-GCE after 5 cycles in **5** and (c) bare Teflon®. At 0.2 V vs. Ag|AgCl.

Five cycles of grafting of **5** on the GCP were sufficient to completely block the electrode surface, as shown by the approach curves towards the grafted surface (Fig. 4.4 (b)) almost matching that seen with the approach to the purely insulating Teflon®, Fig. 4.4 (c). The results confirm the observations made for CV, in Fig. 4.3.

The area scan technique was also used to analyse the grafted surface. The analysis was carried out on a GCP, with attempts made to show the difference in the surface by scanning over the interface of where grafting was done and not done, as well as scanning over the edge of the plate to show a comparison between the surface and the bulk medium. To generate this type of data the GCP plate was not completely grafted over its whole surface in order to afford an interface region for comparison in most cases, but in some cases the whole plate is grafted for completeness.

Figure 4.5 shows the SECM images of the GCP at an interface region where unmodified and grafted surface conductivity can be visualised, Fig. 4.5(a). In Fig. 4.5(b) almost the whole GCP

was scanned and in this case the whole plate was grafted to show uniformly that it is less conductive than the bulk medium, as shown in the approach curves. Fig. 4.5(c) shows the whole GCP again from a different angle and here the noise that shows up as vibrations from an air conditioner stationed in the lab are very clear. The air conditioner is barely detectable by touch of the hand to the table top where the SECM instrument sits but the sensitivity of the technique is well illustrated. A photograph is also shown in Fig. 4.5(d) to illustrate how the surface is imaged as a function of conductivity but this still shows surface defects and the physical shape of the GCP itself and even areas where the GCP has been chipped as a result of being dropped or damaged during use.

(a)

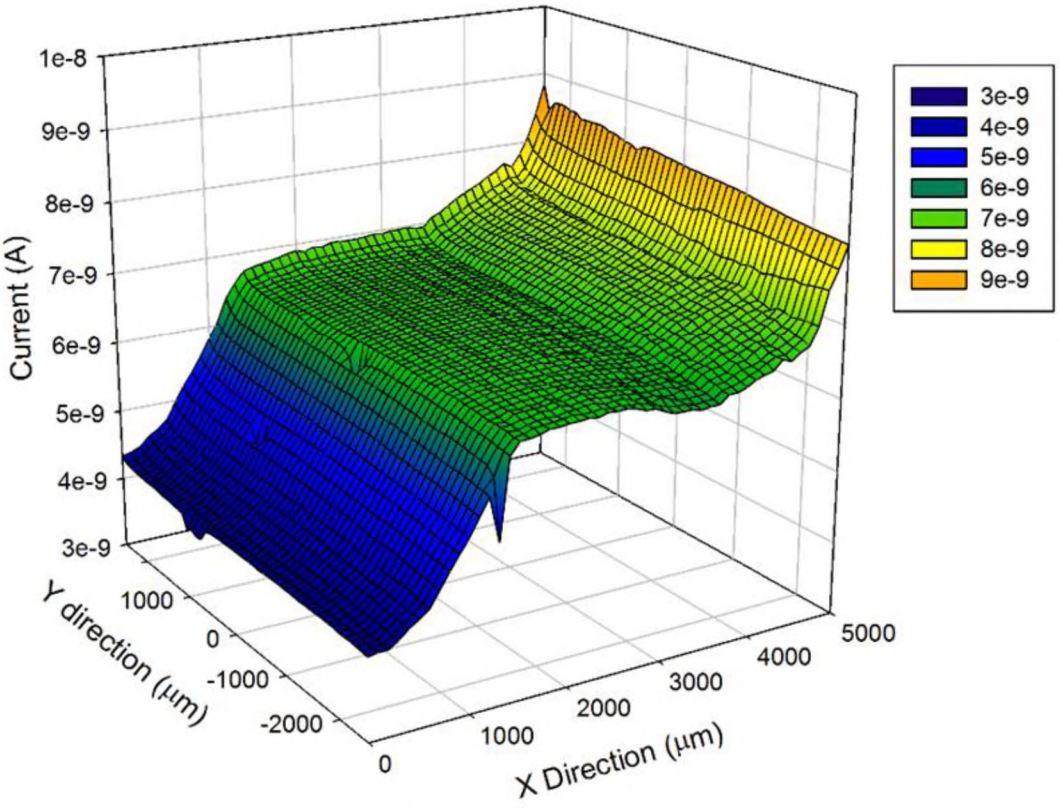
1e-8
9e-9
8e-9
7e-9
6e-9
5e-9
4e-9
3e-9
Current (A)
3e-9
4e-9
5e-9
6e-9
7e-9
8e-9
9e-9
1000
0
-1000
-2000
Y direction (µm)
0
1000
2000
3000
4000
5000
X Direction (µm)

(b)

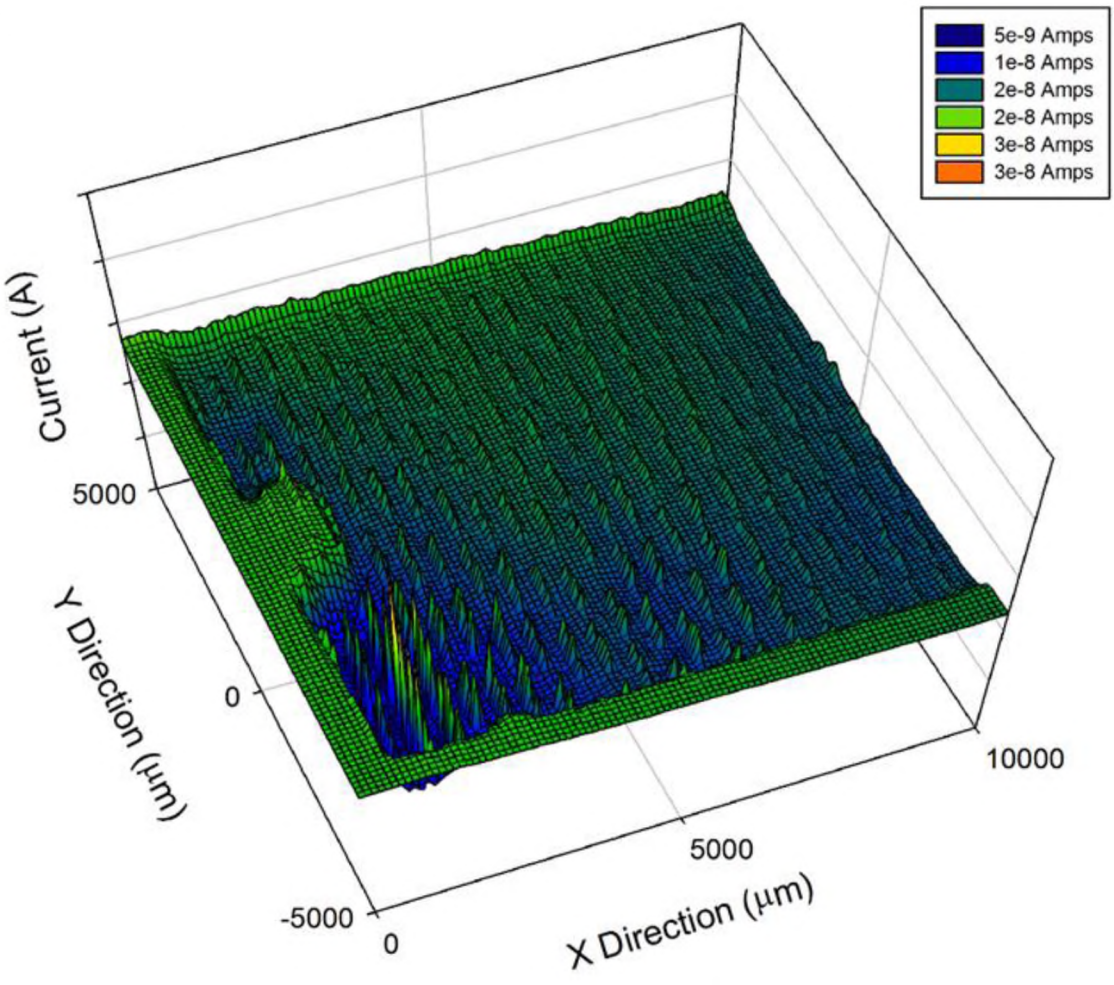
5e-9 Amps
1e-8 Amps
2e-8 Amps
2e-8 Amps
3e-8 Amps
3e-8 Amps
Current (A)
5000
0
-5000
Y Direction (µm)
0
5000
10000
X Direction (µm)

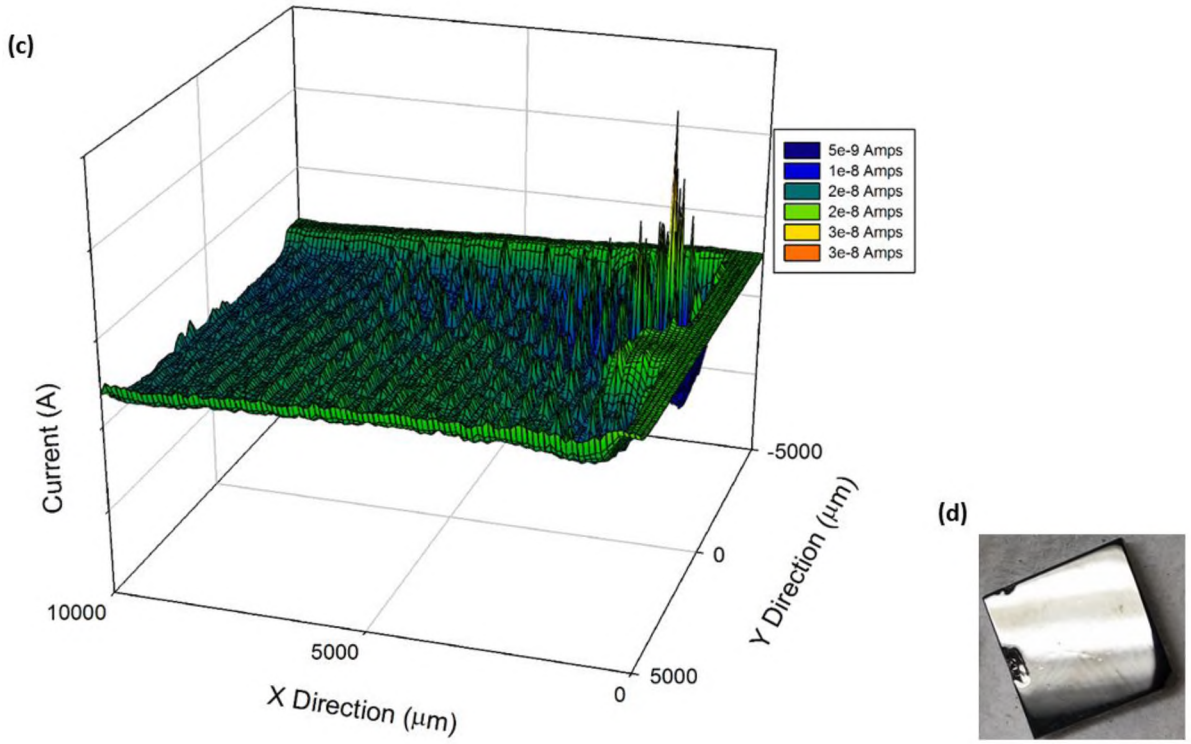

Figure 4.5. SECM images of (a) an interface region, where the blue (less conductive) section shows the grafted area and the green to orange (more conductive) area shows the merging of the interface into an unmodified, bare area. Part (b) shows a large area scan where almost the whole surface of the GCP is imaged and surface physical defects are visible, as well as the edge of the GCP, showing how the grafted surface is less conductive than the bulk medium. Part (c) shows another angle with the data from (b), chosen to show the noise generated by external vibrations. Part (d) is a photograph of the actual GCP that was used in these scans, shown to illustrate how directly the GCP is imaged and that physical dimensions can be visualised through changes in conductivity. All images taken with a 25 µm diameter Pt UME in 5mM $K_4[Fe(CN)_6]$ in 0.1 M KCl (E_{tip} = 0.2 V vs. Ag|AgCl). The tip was scanned at 10 µm / s.

4.1.3 XPS characterisation

The final technique used to characterise the grafted surface was XPS. The high-resolution scanning capability of the XPS is very powerful and thus useful in showing the presence of the grafted azide groups on the surface. The central nitrogen group of the azide has a distinctive peak at higher binding energy than the adjacent nitrogen groups [67,76,78,99]. The ratios of the peaks are expected to be 1:2 [99], but deviations from this ratio have been reported in certain cases [76,78,100], and are attributed to degradation of the azide as a result of

undergoing lengthy analysis under XPS conditions [75], and also to some residual nitrogen from the underlying surface or solvent.

The grafted GCP was used for these studies. High resolution XPS of the N (1s) region of the surface is shown in Fig. 4.6. A peak was observed at ~404 eV, which is attributed to the central nitrogen of the azide, as mentioned previously. The presence of this peak means the grafting of the GCP was successful and thus so was the modification of the GCE.

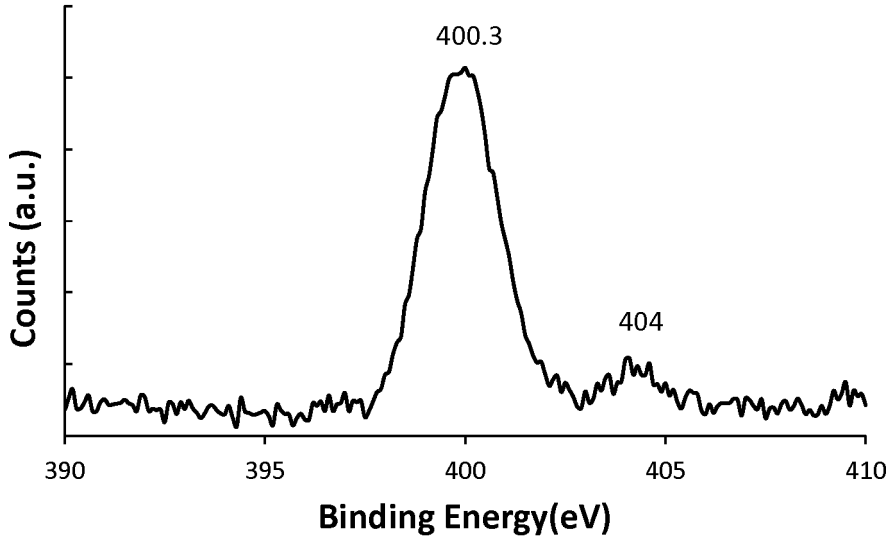

Figure 4.6. High resolution XPS of the N (1s) region of the GCP after grafting for three cycles using **5**. Pass energy = 80 eV, number of sweeps = 5.

The peak signal at ~400.3 eV is due to the overlapped peaks of the adjacent nitrogen groups in the azide functionality [75,99].

4.2 Click chemistry attachment of Pcs

Following electrochemical grafting with **5**, the grafted GCE was further modified through click chemistry. This process follows the step-wise modification approach of graft-then-click, as shown in Scheme 4.2. The same methods of characterisation as were employed for the grafted layer were used for the characterisation of the clicked layer of Pcs on the surface of the electrodes - electrochemistry, SECM and XPS. XPS was very valuable as it could be used to follow the success of the click reaction by following the disappearance of the azide signal [67,76,78,100], and as used before, the conductive or insulating nature of the surface was confirmed with SECM [84,101].

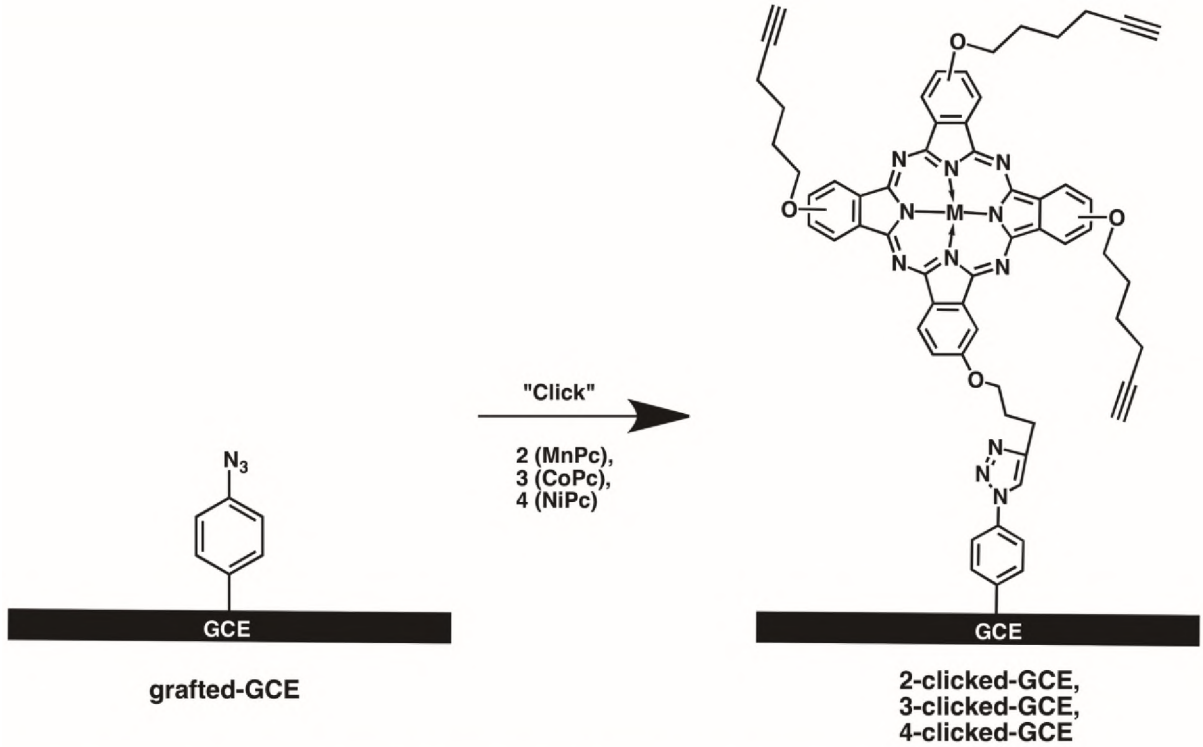

Scheme 4.2. Proposed click chemistry attachment of complexes **2**, **3**, and **4**.

Following the grafting step, the click reaction (Scheme 4.2) was performed by immersing the grafted electrode into a solution containing 0.1 µM **2** or **3** or **4** in 5mL DMF containing 2 mM $Cu(PPh_3)_3Br$ and 2 ml triethylamine. The electrode was left to 'click' with complexes **2** or **3** or **4** for 18 h, represented as **2**-clicked-GCE or **3**-clicked-GCE or **4**-clicked-GCE. Copper (II) salts are often purer and less costly than the copper (I) species [60]. The Cu (I) catalyst is responsible for the click chemistry reaction, through the production of a regiospecific 1, 2, 3

– triazole link between the surface groups and the alkyne-bearing compound [59,60,65,68,102]. The trimethylamine acts as a base.

Attachment of alkyne substituted Pcs has been achieved before through click chemistry with the azide groups on a GCE [15]. However, this is the first time a series of metals have been compared through the use of this approach, as outlined in Scheme 4.2.

4.2.1 Cyclic voltammetric characterisation

Pcs are very useful complexes to attach to the grafted surface as they have strong redox activity and thus, once covalently attached to the modified electrode, electrochemical characterisation can be used to prove attachment. The grafted electrodes retained their blocking characteristics towards ferrocyanide following click chemistry as shown in Fig. 4.3. The stepwise method of electrode modification was chosen above alternate methods such as click-then-graft as the graft-then-click approach has been shown to be more effective in maximising the attachment of the complexes to GCE surfaces, without a loss in electroactivity during the modification process [103].

4.2.2 SECM characterisation

Fig. 4.7 shows the approach curves to the GCP with bare, grafted and clicked with each complex **2**, **3** and **4** to compare the behaviour after click chemistry. Fig. 4.7 shows the approach curve results for grafting and click chemistry on the GCP. Following click chemistry, the SECM probe still showed negative feedback response upon approach to the modified surface, Fig. 4.7 (c–e), indicating that the grafted layer was still present and that the click chemistry conditions did not greatly affect the blocking capability of the electrode. In the case of **2**-clicked-GCP and **3**-clicked-GCP there was even an enhancement of the negative feedback while with **4**-clicked-GCP there was a decrease in the insulating characteristics.

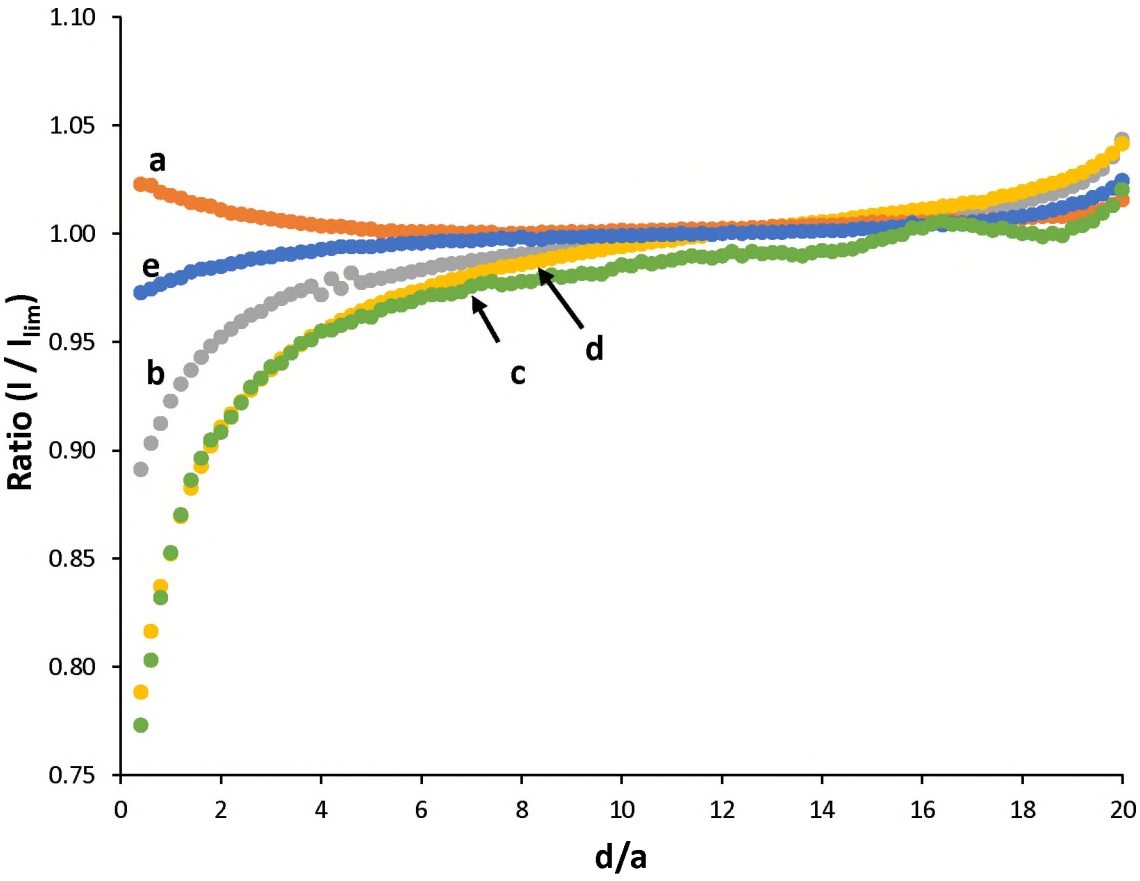

Figure 4.7. SECM approach curves using 25 µm Pt UME in 5mM $K_4[Fe(CN)_6]$ in 0.1 M KCl. Approach to (a) bare-GCP, (b) grafted-GCP after 5 cycles in **5**, (c) **2**-clicked-GCP, (d) **3**-clicked-GCP and (e) **4**-clicked-GCP. At 0.2 V vs. Ag|AgCl.

The Pcs, although electrochemically active themselves, did not catalyse the oxidation or reduction of the ferrocyanide. The slight increase in insulating characteristics shown by **2**-clicked-GCP and **3**-clicked-GCP can be attributed to the formation of another layer on the substrate, which would further limit the diffusion of the redox analyte to the GCP surface and slow electron transfer. The reason behind **4**-clicked-GCP not showing the same decrease in insulating behaviour could be due to an inconsistent approach curve, whereby the tip did not get as close to the insulating surface as it did with **2** and **3**-clicked-GCPs and thus the redox processes were not as significantly hindered. It is also difficult to replicate the exact same scan to exact same distance from the surface for each step of modification as the GCP is cleaned in between each and hence, can change slightly and induce variation as is observed. What is of significance is that the blocking effect is retained and is still confirmed by observations made and shown in Fig. 4.7.

The blocking effect at the surface, as a result of modification, was monitored with the use of SECM area scans and the GCP was imaged at each stage to generate a comparison of the different layers. All five layers were imaged as they were for the approach curves, but the results of interest are **2**-clicked-GCP, **3**-clicked-GCP and **4**-clicked-GCP thus, the area scans of these surfaces are shown in Fig. 4.8.

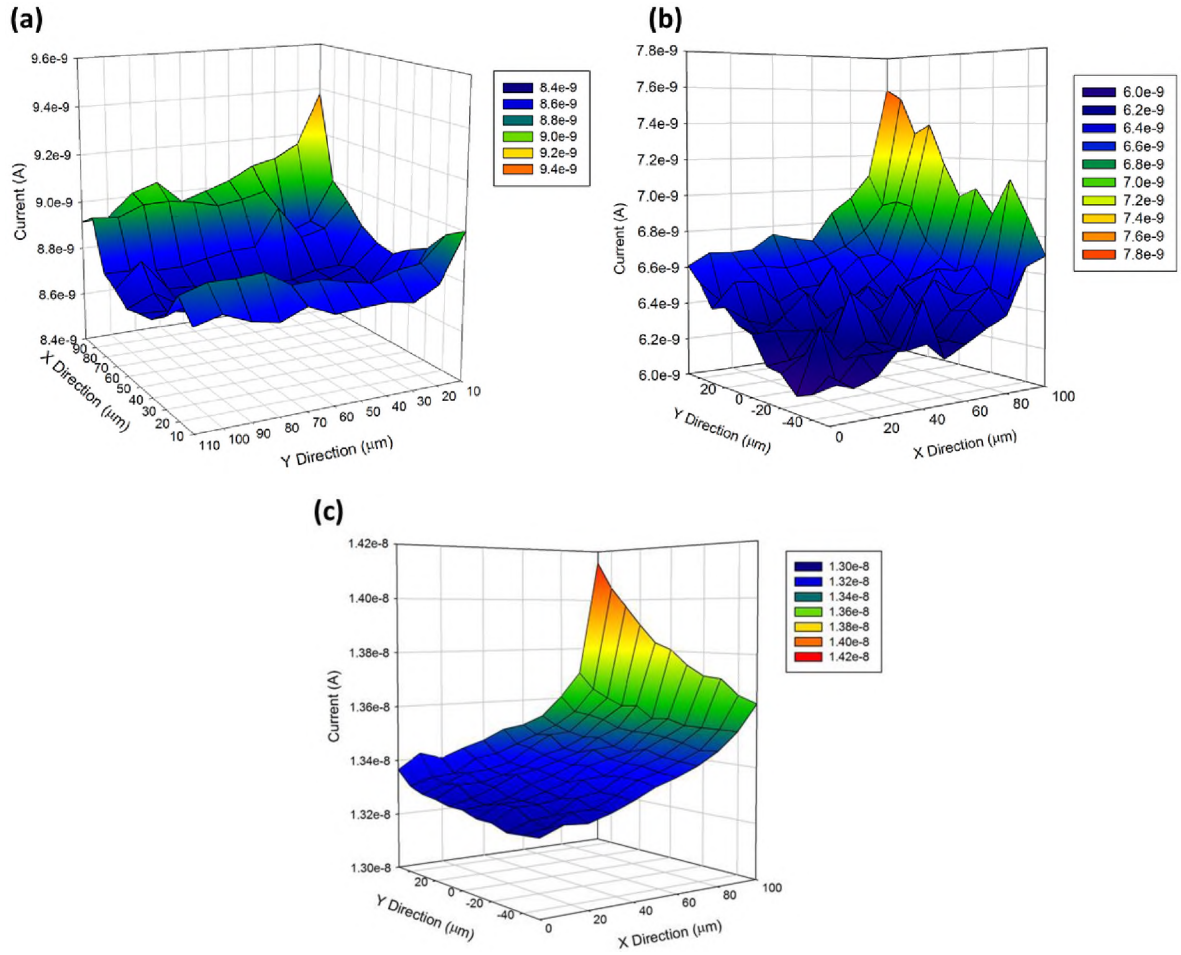

Figure 4.8. SECM images of the GCP following grafting and click chemistry with (a) complex **2** and (b) complex **3** and (c) complex **4**. Imaged with a 25 µm diameter Pt UME in 5 mM $K_4[Fe(CN)_6]$ in 0.1 M KCl, E_{tip} = 0.2 V vs. Ag|AgCl. The tip was scanned at 10 µm / s.

The three images shown in Fig. 4.8 show a change in the blocking effect observed. Fig. 4.8 (a) shows the low average current of approximately 8.4×10^{-9} A after grafting and click chemistry with complex **2**. In Fig. 4.7 (b) where the surface had undergone grafting then click chemistry with complex **3** a lower average current is observed of approximately 6.2×10^{-9} A. Fig. 4.8 (c) shows the slightly increased current average of approximately 1.3×10^{-8} A after grafting and click chemistry with complex **4**. In comparison to the average current observed at the surface of the bare-GCP, which had a value of 1.6×10^{-8} A, all the clicked surfaces exhibit the blocking

effect by showing a reduction in average current compared to the bare-GCP, but to varying degree. The surfaces show a correlation with the approach curve results, as the surfaces clicked with complexes **2** and **3** show a higher blocking effect and therefore, lower average current, than the surface clicked with complex **4**. Complex **4** surface showed minimal reduction in current when compared to that of the bare possibly due to the nature of the experimental setup, as the tip is lowered and positioned manually above the surface each time. In the case of the complex **4** surface, the manual adjustment may have not been as precise and as a result was not able to illustrate the blocking effect as significantly as the surfaces of complexes **2** and **3**.

4.2.3 XPS characterisation

High resolution XPS scans of the N (1s) region following grafting with **5** has been discussed in the previous section and the presence of azide groups on the surface gave distinctive peaks in the XPS spectra. The most useful XPS observation for click chemistry is the disappearance of the peak at higher binding energy in the N (1s) region (at ~404-403 eV, indicative of the presence of the azide) is considered to be evidence of successful click chemistry to form the 1, 2, 3 – triazole link, where all the nitrogen groups are in the same chemical environment [68,76–78,100]. After the click chemistry step, Fig. 4.9 shows the decrease in the peak at ~404 eV at all surfaces and a shift in the largest peak, near 400 eV, to slightly lower energies compared to the grafted surface. Shifts in binding energies in XPS spectra are considered to be indicative of a change in chemical environment [99], and can be assigned here to a change in bonding following the click reaction to form the triazole ring. The data in Fig. 4.9 shows the general trend described as well as a general reduction in the intensity of the nitrogen peaks as a result of the click chemistry, suggesting a layer has been added to the surface. The XPS spectra for **2**-clicked-GCP (Fig. 4.9 blue) showed the peaks of interest at 399.9 eV and a less intense and broad peak at 403.0. The spectrum obtained for **3**-clicked-GCP (Fig. 4.9 (b)) is a very successful indication of the click chemistry inducing the loss of the 404 eV peak as well as a minor shift in the 400 eV peak from 400.4 to 400.3 eV. Finally the spectra obtained for **4**-clicked-GCP (Fig. 4.9 (c)) showed a reduction in the 404 eV peak and a reduction in intensity of the 400 eV peak, as well as a shift, which indicates a change in the chemical environment at the surface.

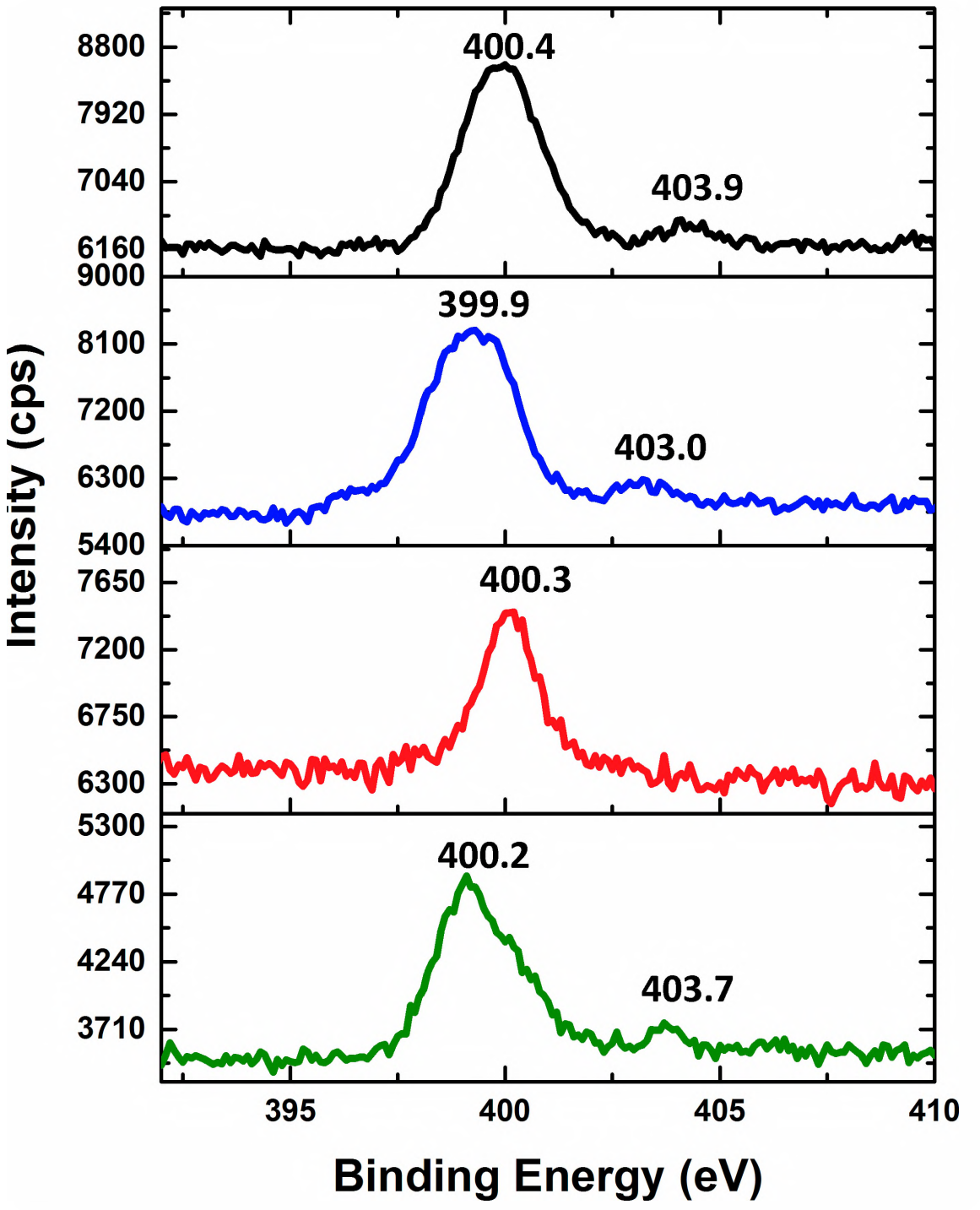

Figure 4.9. High resolution N (1s) XPS spectra for: black: grafted-GCP, blue: **2**-clicked-GCP, red: **3**-clicked-GCP and green: **4**-clicked-GCP. Pass energy = 80 eV, number of scans = 5.

In conclusion, the electrodes, GCE and GCP, were successfully modified and examined with cyclic voltammetry, SECM and XPS. The surfaces were monitored at each step of the modification process from bare-GCE/GCP to grafted-GCE/GCP and finally to **2**-, **3**- and **4**-

clicked-GCE/GCP. Cyclic voltammetry studies showed the blocking effect induced by grafting towards $K_4[Fe(CN)_6]$ and this was substantiated by the SECM studies, which also showed the blocking effect was present on the GCPs. Finally, XPS was used to confirm the modification of the GCP with grafting and then to confirm the attachment of the complexes to the surface via click chemistry.

CHAPTER 5

ELECTROCATALYTIC STUDIES OF HYDRAZINE

5.1 Cyclic voltammetry

5.1.1 Peak potential variation

The methods used to assess the modification approach used in the attachment of **2**, **3**, and **4** to the electrode surface did not show particularly discernible differences between these three surfaces. Hence, the effect of the different metal centres has not yet been fully observed. This section aims to investigate the direct effect of the metal centres by using the three surfaces, **2**-clicked-GCE, **3**-clicked-GCE, and **4**-clicked-GCE to catalyse hydrazine. Hydrazine was chosen as a test analyte as it is well known and the electrocatalysis of hydrazine by phthalocyanines is understood and has been studied in many cases [1,85,104–108]. This electrocatalysis was also used to confirm attachment of the three complexes to the surface of the GCE, as neither the bare-GCE nor the grafted-GCE detected hydrazine in the potential window used (-0.3 – 1.0 V) (Fig. 5.1 (A) (a, b)). However, an electrocatalytic response was observed after click chemistry with the three complexes on the GCE (Fig. 5.1 (A) (c–e)). A clear oxidation process was visible on the anodic scan for all three surfaces, at 0.34, 0.72 and 0.75 V for **2**-clicked-GCE, **3**-clicked-GCE and **4**-clicked-GCE, respectively (Table 5.1), while no peak was observed for the cathodic scan. A CV of **2**-clicked-GCE in 0.2 M NaOH (Fig. 5.1 (B)) demonstrates that the clicked surfaces do not show a peak for the attached Pcs. Hence, surface coverage could not be calculated. **3**-clicked-GCE and **4**-clicked-GCE behaved in a similar manner, not shown.

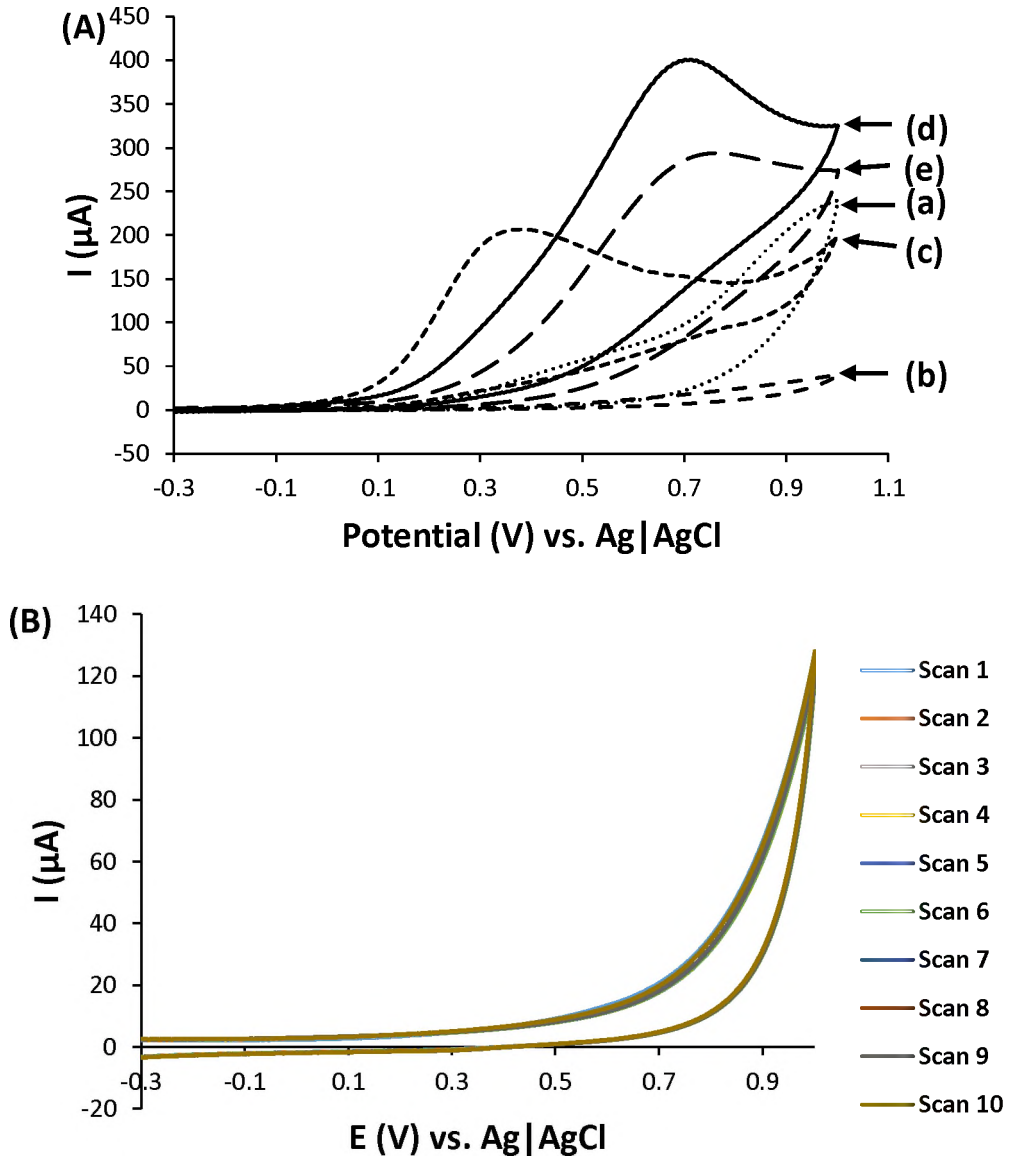

Figure 5.1. (A) Cyclic voltammograms of (a) bare-GCE, (b) grafted-GCE, (c) **2**-clicked-GCE, (d) **3**-clicked-GCE and (e) **4**-clicked-GCE in 6 mM hydrazine monohydrate in 0.2 M NaOH at 100 mV / s vs. Ag|AgCl (3 M KCl). (B) Plots of repetitive scans of **2**-clicked-GCE, as an example, in 0.2 M NaOH alone.

5.1.2 Tafel slopes and mechanism

Fig. 5.2. (a) shows the results of the scan rate studies in hydrazine of complex **2** (MnPc). Fig. 5.2. (b) and 5.2. (c), show linear plots of current vs. square root of scan rate, and peak potential vs. log scan rate for hydrazine oxidation, respectively. The plots in Fig. 5.2. (b) confirm that the catalytic oxidation of hydrazine is diffusion controlled due to the linearity of the plot. The Tafel slopes were calculated using Eqn. 5.1 [109] and the plot shown in Fig. 5.2. (c), to yield 0.472 V / decade for **2**-clicked-GCE. Tafel slopes are calculated for the purpose of gaining insight into the kinetics of the electrochemical reaction and are only applicable if they are linear when on a logarithmic scale [71]. The Tafel slopes for the other two surfaces were found to be 0.212 V / decade for **3**-clicked-GCE and 0.217 V / decade for **4**-clicked-GCE, Table 5.1.

$$E_p = \frac{b}{2} log v + K \tag{5.1}$$

where b is the Tafel slope.

High Tafel slope values above the normal 60-120 mV / decade have no kinetic meaning and are related to electrochemical steps or to substrate-catalyst interactions in a reaction intermediate [110,111]. Therefore, it was difficult to assign which mechanism each complex follows, but based on the activity observed, it was considered reasonable to apply the same assignments as ascribed in literature. The mechanism in Eqn. 5.2–5.5 is the mechanism followed by complex **2** (Mn) and **4** (Ni), according to literature [104,105]. Zagal and others have reported that MnPcs produce the same Tafel slopes (ca. 40 mV / decade) as FePc derivatives [90,105,112] and, as a result, have grouped the two together [105]. Following that, Zagal *et al.* have reasoned that the presence of high Tafel slopes, above 120 mV / decade, is also grounds to assign the FePc mechanism to NiPc derivatives, together with other speculations about acid-base interactions [105].

Iron as central metal mechanism [90]:

$$[Fe(I)PcR_n]^-_{surface} \rightleftharpoons [Fe(II)PcR_n]_{surface} + e^- \tag{5.2}$$

$$[Fe(II)PcR_n]_{surface} + N_2H_4 + 2OH^- \xrightarrow{rds} [Fe(I)PcR_n \dots N_2H_2]^-_{surface} + 2H_2O + e^- \tag{5.3}$$

$$[Fe(I)PcR_n \dots N_2H_2]^-_{surface} \rightarrow [Fe(I)PcR_n]^-_{surface} + *N_2H_2 \tag{5.4}$$

$$*N_2H_2 + 2OH^- \xrightarrow{fast} N_2 + 2e^- + 2H_2O \tag{5.5}$$

According to literature, the mechanism depicted in Eqn. 5.6–5.9 has been assigned to CoPc derivatives. A different mechanism was assigned to CoPc derivatives as they generated higher Tafel slopes (60 mV / decade) than their FePc derivatives. Therefore, in this work, the mechanism shown in Eqn. 5.6–5.9 has been assigned to complex **3**.

Cobalt as central metal mechanism [90]:

$$[Co(I)PcR_n]^-_{surface} \rightleftharpoons [Co(II)PcR_n]_{surface} + e^- \quad (5.6)$$

$$[Co(II)PcR_n]_{surface} + N_2H_4 + OH^- \xrightarrow{rds} [Co(I)PcR_n \dots N_2H_3]^-_{surface} + H_2O \quad (5.7)$$

$$[Co(I)PcR_n \dots N_2H_3]^-_{surface} \rightarrow [Co(I)PcR_n]^-_{surface} + *N_2H_3 \quad (5.8)$$

$$*N_2H_3 + 3OH^- \xrightarrow{fast} N_2 + 3e^- + 3H_2O \quad (5.9)$$

Note: the * indicates a radical specie.

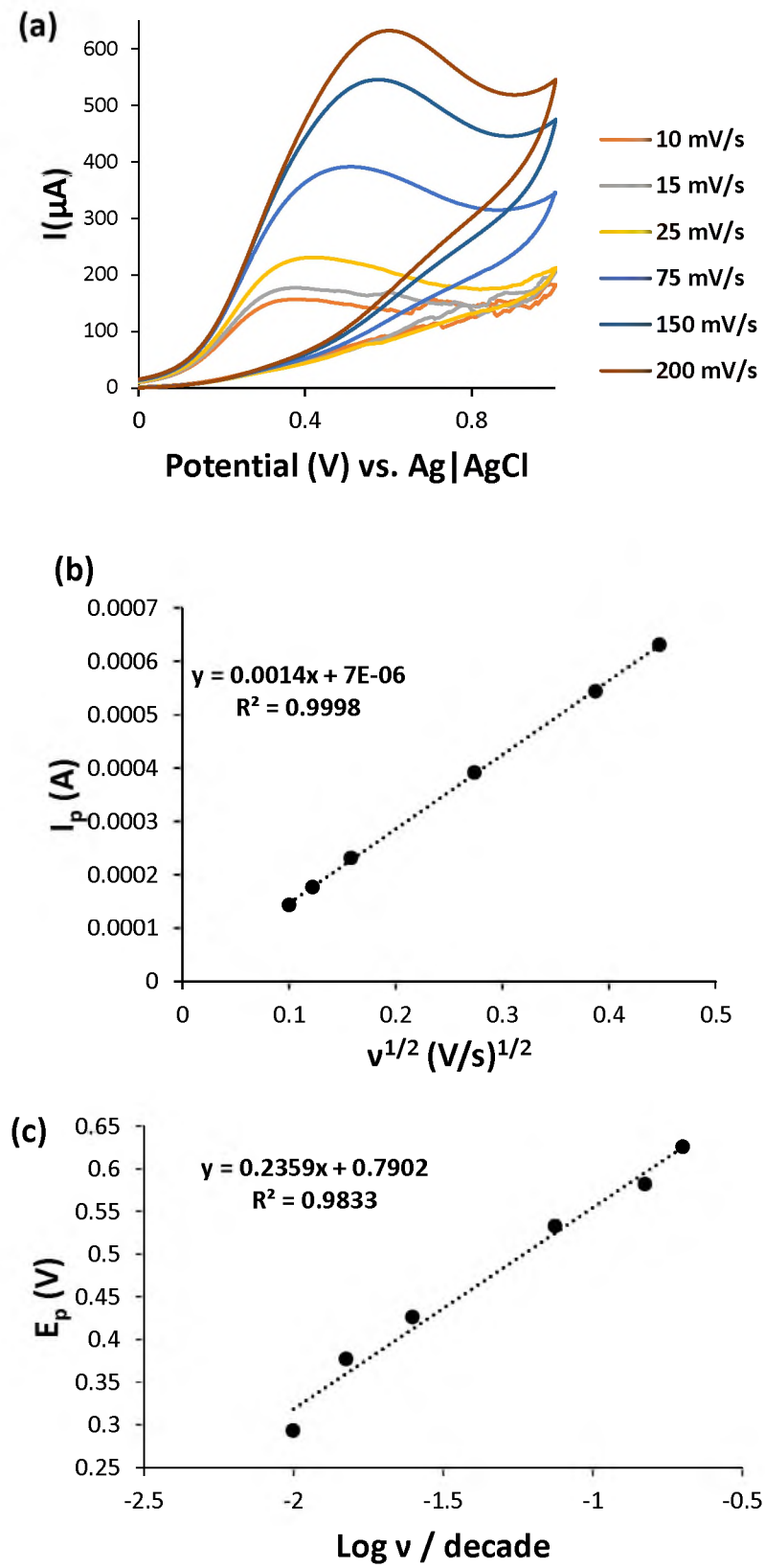

Figure 5.2. (a) Scan rate studies of **2**-clicked-GCE in 6mM hydrazine monohydrate in 0.2 M NaOH at 10, 15, 25, 75, 150 and 200 mV / s. (b) Plots of current vs. square root of scan rate for **2**-clicked-GCE. (c) Plots of potential vs. log of scan rate for **2**-clicked-GCE.

5.1.3 Stability

In the field of electrochemical sensing and in electrocatalysis it is of significance to observe if a modified surface can produce reproducible electrochemical responses [1]. Therefore, a stability test is performed to test how repeatable the electrochemical responses are for a modified surface. Stability was tested by running ten consecutive scans of the clicked surfaces in 6 mM hydrazine in 0.2 M NaOH, Fig. 5.3. There is a decrease in current until approximately the 5th scan for all surfaces; thereafter, the current stabilises. The current of **2**-clicked-GCE (MnPc derivative) stabilises the quickest and with least deviation from the stable peak current. This behaviour is closely followed by **3**-clicked-GCE (CoPc derivative), except for an initial scan that is 50 µA above the rest. Finally, the **4**-clicked-GCE (NiPc derivative) shows the slowest stabilising behaviour. For comparison sake, as an example of the benefits of the click modification method, complex **3** was adsorbed onto the GCE and tested for stability (Figure 5.3 (d)). The adsorbed method produces a surface that loses current carriage with each consecutive scan, proving to be less stable than its clicked counterpart.

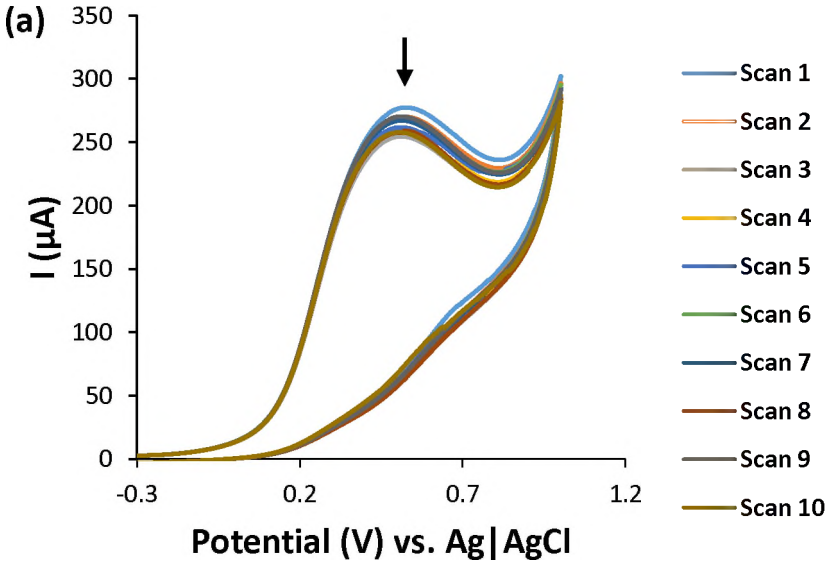

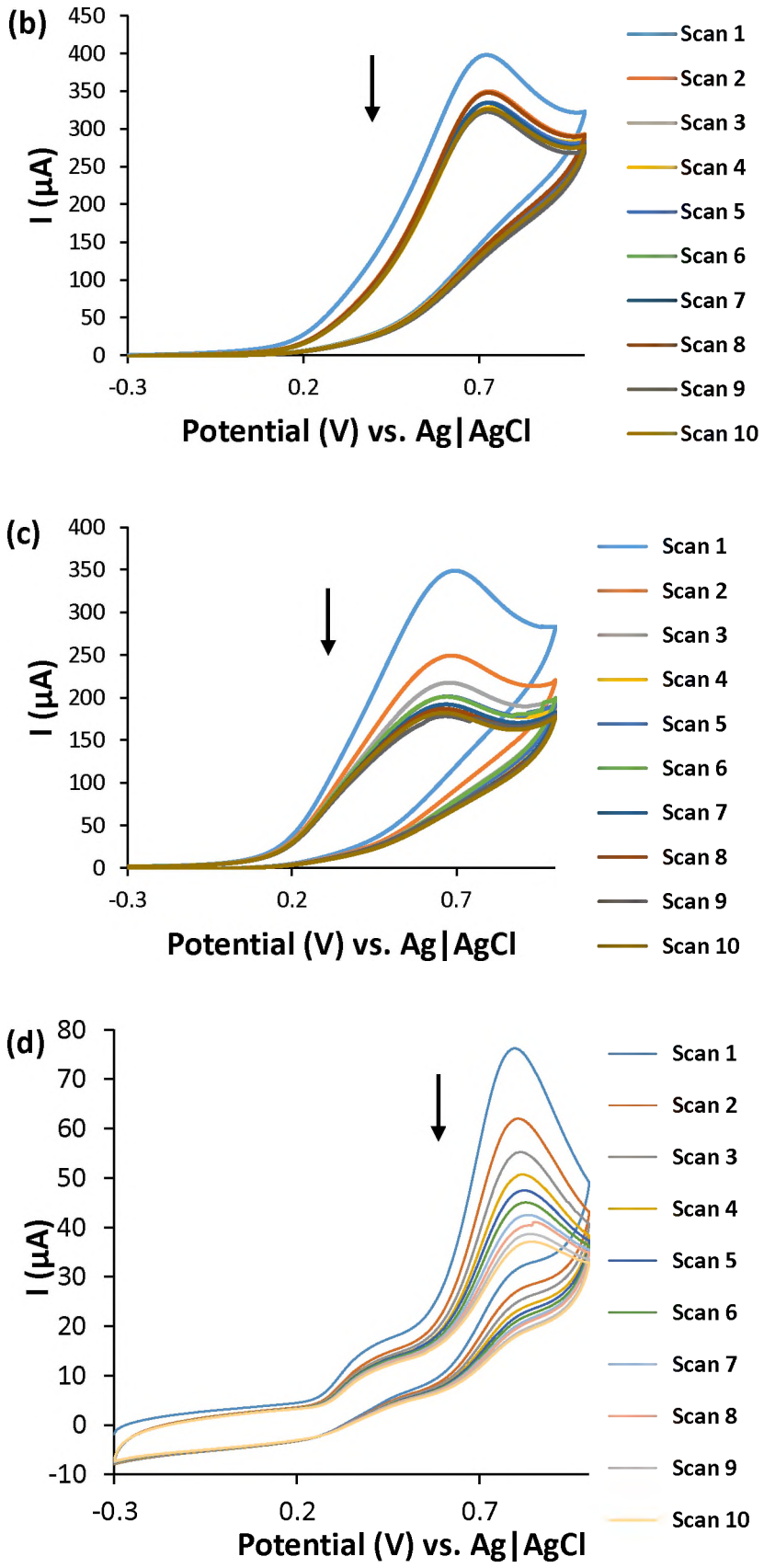

Figure 5.3. Plots of repetitive scans of (a) **2**-clicked-GCE, (b) **3**-clicked-GCE and (c) **4**-clicked-GCE (d) **3**-adsorbed-GCE in 6mM hydrazine in 0.2 M NaOH.

5.2 Electrochemical impedance spectroscopy (EIS)

EIS was used to determine the charge transfer resistance (R_{CT}) and to give information on the electron transfer kinetics in the presence of hydrazine. The charge transfer resistance is a representation of how fast an electron exchange occurs at the electrode surface and therefore, the impact of a modification that improves this electron exchange (electrocatalysis) can be observed through the R_{CT} [71]. In essence, if the R_{CT} is lowered it represents an increase in charge transfer and hence, proof of electrocatalysis. Fig. 5.4 shows the Nyquist and Bode plots for the bare- and grafted-GCE, as well as the three clicked surfaces. The diameter of the semi-circle in the Nyquist plot gives the charge transfer resistance (R_{CT}). All five surfaces exhibited the characteristic semi-circle (Fig. 5.4. (A) (a–c)) with the following R_{CT} values: bare-GCE: 9.77 kΩ (average of all three); grafted-GCE: 7.27 kΩ (average of all three); **2**-clicked-GCE: 1.13 kΩ; **3**-clicked-GCE: 1.55 kΩ; **4**-clicked-GCE: 2.60 kΩ, Table 5.2.

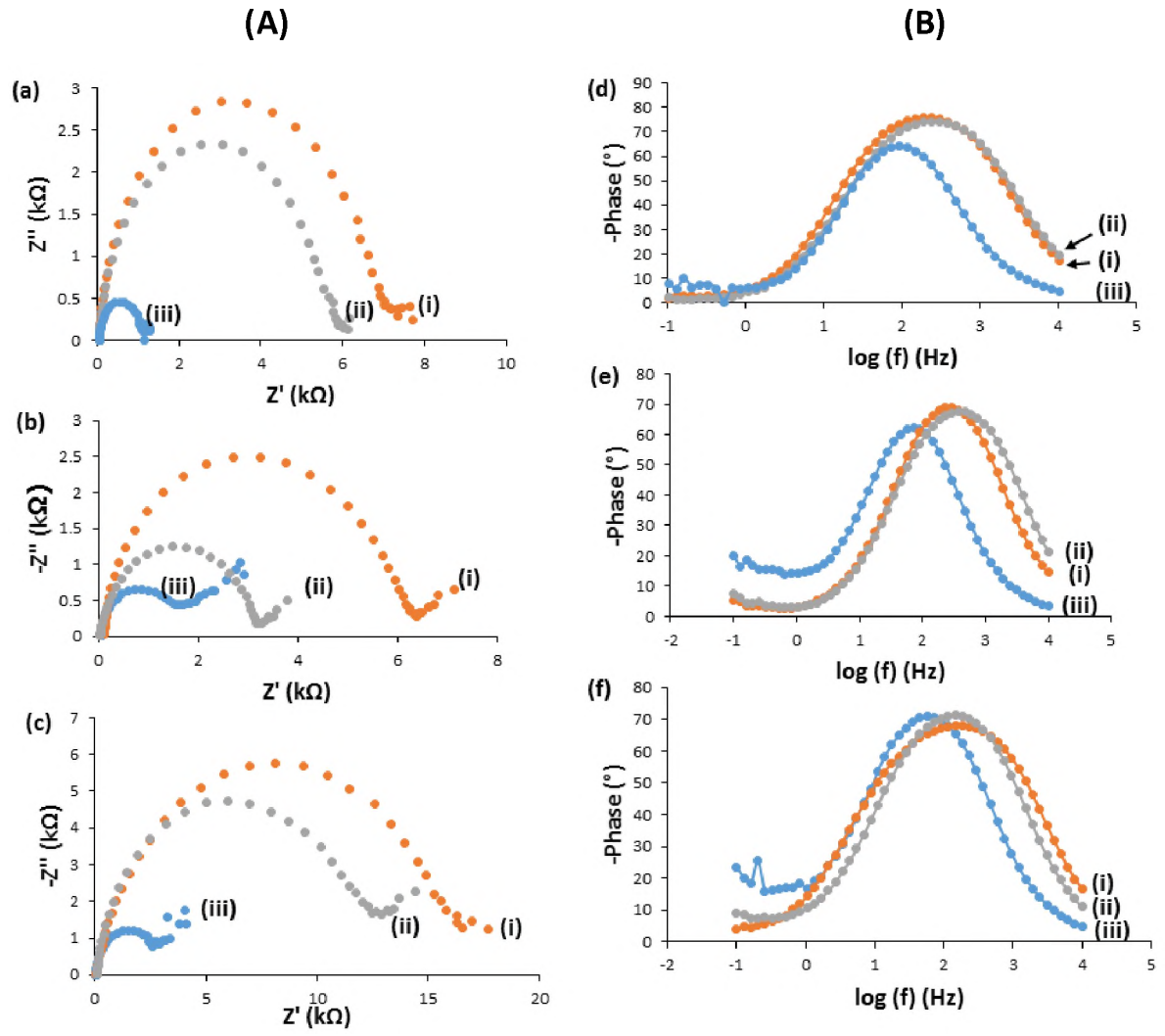

Figure 5.4. (A) Nyquist plots and (B) Bode plots for (a) **2**-clicked-GCE, (b) **3**-clicked-GCE and (c) **4**-clicked-GCE, where (i) is bare surface, (ii) is grafted surface and (iii) surface after click chemistry. All scans recorded in 6 mM hydrazine in 0.2 M NaOH.

This shows that the **2**-clicked-GCE has the most conductivity, or least resistance, with **3**-clicked-GCE following closely. **4**-clicked-GCE had the least conductivity, or most resistance, when compared to the other two surfaces. This correlates with the CVs of the surfaces in hydrazine solution (Fig. 5.1. (a), Table 5.1.), where **2**-clicked-GCE has the lowest potential for hydrazine oxidation, followed by **3**-clicked-GCE and, finally, **4**-clicked-GCE. This trend proves the attachment of **2**, **3**, and **4**, as it facilitates improved electron transfer at the surface.

The apparent electron transfer rate (K_{APP}) for each surface is obtained using Eqn. 5.10 [113]:

$$K_{APP} = \frac{RT}{F^2 R_{CT} C} \tag{5.10}$$

where 'C' is the concentration of the hydrazine (mol / L), 'R' is the universal gas constant (J / mol. K), T is temperature (K), 'F' is Faraday's constant (96485 C / mol) and 'R_{CT}' is charge transfer resistance. Calculated values of K_{APP} are as follows: bare-GCE: 5.37 × 10^{-9} cm / s (average of three); grafted-GCE: 8.42 × 10^{-9} cm / s (average of three); **2**-clicked-GCE: 4.03 × 10^{-8} cm / s; **3**-clicked-GCE: 2.85 × 10^{-8} cm / s; **4**-clicked-GCE: 1.71 × 10^{-8} cm / s. Again, the **2**-clicked-GCE showed indications of a higher electron transfer by having the largest K_{APP} value, followed by **3**-clicked-GCE and, finally, by **4**-clicked-GCE.

A plot of phase-shift vs. log frequency (Fig. 5.4. (B) (a–c)) provides extra information on frequency, which cannot be obtained from the Nyquist plot. The phase angle values for all the electrode surfaces studied in this work are less than the ideal 90° for a true capacitor [114]. Changes in phase angles and frequencies are unambiguous indications of the structural differences of the surfaces, and indicate that oxidation of the analyte occurred at the modified surfaces rather than on the bare GCE. The phase angle changes from 71.0° (average of three) for the bare-GCE to 70.8° (average of three) for the grafted-GCE and then to 62.5° for the **2**-clicked-GCE, 61.6° for the **3**-clicked-GCE, and 70.9° for the **4**-clicked-GCE.

5.3 Chronoamperometry

The three surfaces were tested for their response to hydrazine in chronoamperometry studies; **3**-clicked-GCE, as an example, is shown in Fig. 5.5. The catalytic current (I_{CAT}) is dominated by the rate at which hydrazine is oxidised at the surface of the modified GCE. The rate constant was determined according to Eqn. 5.11 [115]:

$$\frac{I_{CAT}}{I_{BUFF}} = \gamma^{\frac{1}{2}}\pi^{\frac{1}{2}} = \pi^{\frac{1}{2}}(k_{CAT}Ct)^{\frac{1}{2}} \quad (5.11)$$

where 'I_{CAT}' represents the catalytic current, 'I_{BUFF}' represents the current when no hydrazine is present in 0.2 M NaOH solution alone, 'k_{CAT}' is the catalytic rate constant, 'C' is the concentration of hydrazine and 't' is the time elapsed. The I_{CAT} / I_{BUFF} ratios were plotted against the square root of time (Fig. 5.5. (b)), and the slopes from Fig. 5.5. (b) were plotted against the concentration of hydrazine (Fig. 5.5. (c)). A linear relationship was observed and k_{CAT} found to be 8.97×10^3 M^{-1} s^{-1} for **2**-clicked-GCE, 7.85×10^5 M^{-1} s^{-1} for **3**-clicked-GCE and 6.65×10^2 M^{-1} s^{-1} for **4**-clicked-GCE. The **3**-clicked-GCE showed the highest value of all three, followed by **2**-clicked-GCE and, finally, **4**-clicked-GCE. These values give an indication as to how fast each surface breaks down hydrazine and, hence, complex **3** was the fastest, followed by complex **2** and, finally, complex **4**.

Using chronoamperograms at different hydrazine concentrations shown in Fig. 5.5. (a), a calibration curve was generated (Fig. 5.5. (a) (insert)). The limits of detection (LoD) were calculated from the calibration curves and found to be 32.6 µM for **2**-clicked-GCE, 25.5 µM for **3**-clicked-GCE and 51.5 µM for **4**-clicked-GCE, using the 3δ / slope ratio, where δ is the standard deviation of the surfaces in electrolyte (0.2 M NaOH) alone, over 20 scans. The sensitivities of the surfaces were found to be 7.97, 12.1 and 18.6 µA / mM for **2**-clicked-GCE, **3**-clicked-GCE and **4**-clicked-GCE, respectively (Table 5.1).

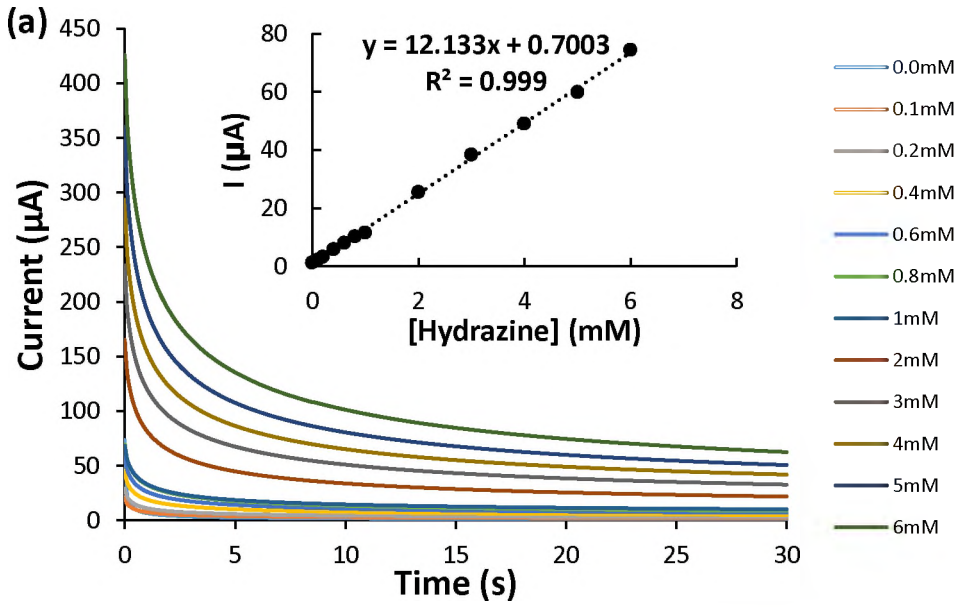
(a)
Current (µA)
Time (s)
I (µA)
[Hydrazine] (mM)
y = 12.133x + 0.7003
R² = 0.999
0.0mM
0.1mM
0.2mM
0.4mM
0.6mM
0.8mM
1mM
2mM
3mM
4mM
5mM
6mM

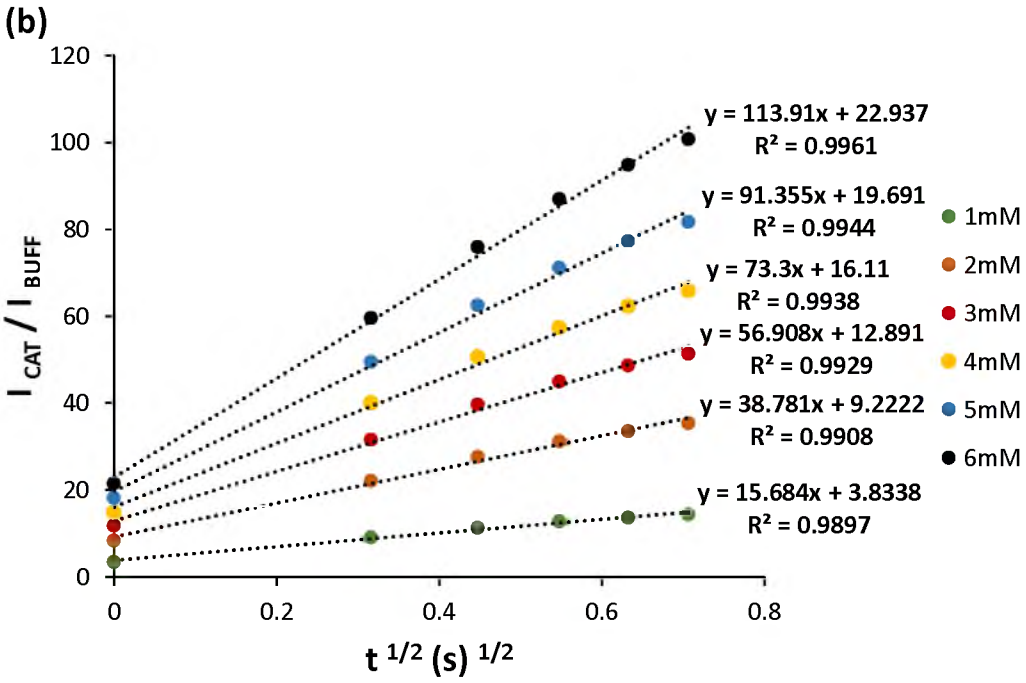
(b)
I CAT / I BUFF
t 1/2 (s) 1/2
y = 113.91x + 22.937
R² = 0.9961
y = 91.355x + 19.691
R² = 0.9944
y = 73.3x + 16.11
R² = 0.9938
y = 56.908x + 12.891
R² = 0.9929
y = 38.781x + 9.2222
R² = 0.9908
y = 15.684x + 3.8338
R² = 0.9897
1mM
2mM
3mM
4mM
5mM
6mM

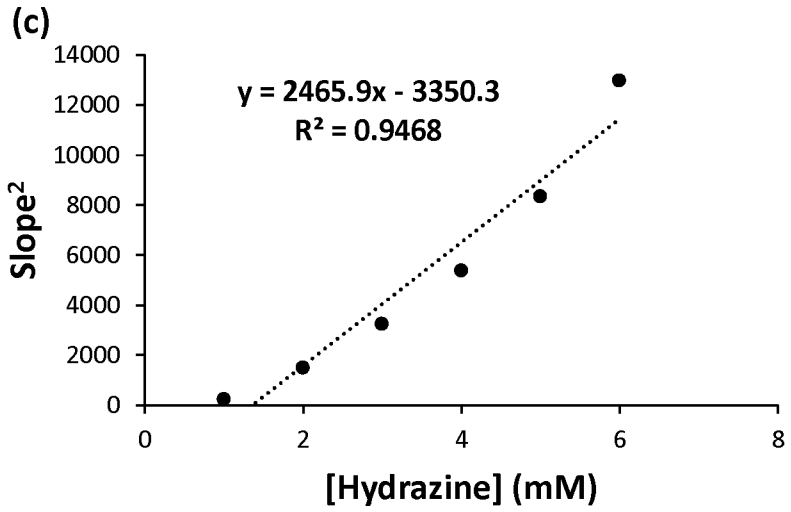

Figure 5.5. Chronoamperometric data collected for the **3**-clicked-GCE surface. (a) Chronoamperometric response to hydrazine at varying concentrations over 30 secs – insert: calibration curve generated from chronoamperometric response, (b) plots of I_{cat} / I_{buff} vs $t^{1/2}$, and (c) plot of the squared slopes from (b) vs. the concentration of hydrazine. All scans carried out in 0.2 M NaOH, concentrations of hydrazine shown in plots.

Hydrazine sensors with MPcs clicked as catalysts follow the trend observed in literature where the MPcs are adsorbed onto the GCE [15,85,90,105]. FePc performs the best with the lowest LoD [15], followed by CoPc, then MnPc and, finally, NiPc (Table 5.1).

5.4 Comparison of surfaces for catalysis of hydrazine

The three surfaces were examined extensively for their catalytic behaviour towards hydrazine. One of the goals of this work is to compare the three surfaces to each other and to literature. While the trends in reactivity of MPcs has been established, this has been achieved using the adsorbed species. This work aims to determine if the same trend is followed for the clicked species.

Table 5.1. Q band absorption wavelengths for the four Pcs that have been investigated by this group. Electrochemical data for **2**, **3** and **4**, together with their FePc counterpart, is shown for comparison sake. Hydrazine concentration is 6 mM unless otherwise stated.

Complex	λ (Q band) nm in DMF	E / V hydrazine oxidation in 0.2 M NaOH	Tafel slopes (mV / decade)	Background corrected currents / μA hydrazine oxidation	Sensitivity (μA / mM)	LoD μM	Ref
2	732	0.34	471	205	7.97	32.6	This work
3	676	0.72	212	399	12.1	25.5	This work
4	674	0.75	217	290	18.6	51.5	This work
FePc derivative	700[a]	0.1	68.5	78[b]	15.38	1.09	[15]

[a] monomeric component, [b] hydrazine at 5 mM.

Table 5.2. Results from EIS investigations for all five surfaces considered in this work. The R_{CT} and k (cm / s) values are shown. The k_{cat} from chronoamperometric data is also shown for the three surfaces. All scans measured in 6 mM hydrazine in 0.2 M NaOH.

Surfacex	R_{CT} (kΩ)	K_{APP} (cm /s)	k_{CAT} (M^{-1} s^{-1})
Bare GCE	9.77	5.37×10^{-9}	-
Grafted GCE	7.27	8.42×10^{-9}	-
2-clicked-GCE	1.13	4.03×10^{-8}	8.97×10^{3}
3-clicked-GCE	1.55	2.85×10^{-8}	7.85×10^{5}
4-clicked-GCE	2.60	1.71×10^{-8}	6.65×10^{2}

The electrocatalytic oxidation of hydrazine at various potentials has been shown with MnPc [90,105], CoPc [28,86,90,104,112,116,117], and NiPc [90,104]. Typically, NiPc derivatives are outperformed by their CoPc and MnPc counterparts in this regard [105]. However, in this work, complex **4** showed comparable catalytic activity to that of complexes **2** and **3**, which has not been previously observed [112], except in the case of Perez *et al.* who reported good activity with silica gel modified with tetrasulfonated NiPc [118]. A number of studies confirming the relationship between the potential of the MPc redox couple and the potential of hydrazine electrocatalysis have been done, proving the involvement of the central metal couple of the Pc [90,104,105,107,112].

The generally accepted mechanism [90,105,119,120] for the electrocatalytic oxidation of hydrazine by MPc complexes begins with the oxidation of the central metal from $M^{I}Pc$ to $M^{II}Pc$ (Eqn. 5.2 and 5.6), followed by electron transfer from the hydrazine molecule to the metal, Eqn. 5.3 and 5.7. Based on the research into the mechanism of the reaction, two different mechanisms have been proposed (Eqn. 5.2-5.9), namely, the FePc mechanism and the CoPc mechanism [85,90,104,105,112]. The Sabatier principle appears to govern the efficiency of the reaction, as there is an exact formal potential that the catalyst should have (ca. -0.5 V vs. SCE [90,105]) for the most successful oxidation of the hydrazine molecule. Zagal *et al.* have speculated that spatial constraints of the orbitals involved in an interaction between the hydrazine molecule and the central metal of the Pc are what govern the order of activity observed for these complexes, and their ability to oxidise hydrazine. However, Zagal *et al.* have also recognised the impact of the electronic structure of the central metal on the trend of activity, which stands as Fe>Co>Mn>Ni in general and in the context of this work [85,90,105]. The hydrazine molecule must form an adduct with the central metal, where the hydrazine acts as an electron donor and the metal acts as an electron acceptor. The formation of this adduct and subsequent electron exchange has been shown for FePc [105], and causes the weakening of the bonds between N and H. The drainage of electrons from the hydrazine molecule into the metal has led to the proposition of two mechanisms because there is either one or two electrons exchanged. However, the order of reactivity remains the same whether there are one or two electrons exchanged. One may have speculated that, due to the higher energy demand of a two-electron exchange, one metal may be favoured over another. This is indeed not the case and, as a result, Zagal *et al.* [105] have explained how the electronic

structure of the central metal affects this electron exchange, in conjunction with calculations made by Taube *et al.* [121]. Zagal *et al.* [105] suggest that the energy of the HOMO $a_{1g}(dz^2)$ in different MPcs decreases almost linearly from MnPc to NiPc. This correlates with the ability of the metal to form adducts with electron donors like hydrazine [105]. One would expect a more favourable (reversible) interaction with Mn, Fe and Co Pcs as they have an empty or half-filled a_{1g} orbital, which has the proper symmetry for the interaction [105]. Indeed, these metals show the highest activity according to literature and this work. The electron drainage from hydrazine upon interaction is not favoured with Ni derivatives since the a_{1g} orbital is filled [105]. It is important for the catalyst to bind with the hydrazine molecule, conduct electron exchange, and then be bound weakly enough to allow the now-radical specie to leave the active site (central metal) again. However, what is of interest is that the order of activity is based on an optimum energy of the HOMO, and not just whether the energy is too low or too high. Therefore, the Sabatier principle provides good rationale for the trend observed in activity of the MPcs.

The mechanism for the oxidation of hydrazine has been subject to change in recent years, with increasing observations of the evolution of nitrogen gas during the oxidation process. The existing mechanism [104,105,112] was brought into question and Zagal and co-workers recently proposed two new mechanisms (Equations 5.2-5.8) that account for the generation of the nitrogen gas, which can often be easily seen at the face of the electrode during a typical CV scan [85,90,122], as was the case in this work.

In Eqn. 5.2 and 5.6 the metal centre must be reduced before it can interact for catalysis. This reduction is typically seen as a peak couple in a CV of the adsorbed MPc in electrolyte solution in the absence of an analyte [105,123]. It is also important that this peak couple occurs before the oxidation point of hydrazine, which would then confirm that couple's involvement in the oxidation [123]. With an adsorption method of modification, the redox couples of MPcs occur at various potentials [104,105,112]. The Mn^{III}/Mn^{II} couple occurs at -0.25 V [35], the Co^{II}/Co^{I} couple occurs at -0.5 V, the Co^{III}/Co^{II} occurs at approximately 0.5 V [111], and the Ni^{III}/Ni^{II} couple occurs at 0.35 V [124]. With the graft-then-click modification approach, it was not possible to see any peak couples when the electrodes were run in the electrolyte alone (Fig. 5.1 B) and, hence, it was not possible to assign a couple for the interaction with hydrazine. Based on the literature, it is believed that the M^{II}/M^{I} couple is the couple involved [90,105]

but, given the positive potential at which the electro-oxidation of hydrazine occurs with the electrodes employed in this work, it is reasonable to speculate the involvement of the M^{III}/M^{II} couples instead of the M^{II}/M^{I} couples. It is also possible the reactions are highly shifted to the right due to high surface concentration of adducts (N_2H_3...$MPcR_n$) brought on by the graft-then-click attachment process [105]. Regardless of which couple is involved, the fundamental mechanism, in which there is electron exchange between the hydrazine molecule and the metal centre of the Pc, still applies.

In Eqn. 5.3 and 5.7, the adduct formation of N_2H_X...$M^{I}Pc^{-}$ is shown. In the FePc mechanism there is an exchange of two electrons, and in the CoPc mechanism there is an exchange of one electron. This is the principle part of the electrocatalysis of hydrazine that leads to the N-H bonds in the compound becoming weakened by the loss of an electron or electrons to the metal centre. This step is the rate determining step.

Eqn. 5.4 and 5.8 show the disassociation of the adduct N_2H_X...$M^{I}Pc$, which releases the reactive radical hydrazine specie back into the bulk solution where it may be oxidised further to nitrogen gas. At this point, the discussion on the influence of the energy of the a_{1g} orbital of the metal shows its rationale, as the Sabatier principle dictates a 'just right' electronic structure affects the efficiency of this part of the mechanism.

Finally, Eqn. 5.5 and 5.9 show the new addition to the mechanism that accounts for the formation of the N_2 gas at the electrode surface. The radical specie generated by the interaction and electron exchange with the metal centre of the Pc is oxidised, quickly, to form nitrogen gas and water. Table 5.1 provides a summary of the peak potentials recorded for each surface and its electrooxidation of hydrazine.

The data presented in Tables 5.1 and 5.2 indicates the presence of a trend in the reactivity of the three surfaces. This trend shows complex **3** as the most effective catalyst for hydrazine, compared to **2** and **4**, when immobilised on an electrode surface via click chemistry. In terms of LoD, the complex **3** surface achieved the best LoD and the highest k_{CAT}, despite the higher potential observed, as the lowest potential (closest to zero) is typically the most effective due to the reduced overpotential. The MnPc derivative, complex **2**, showed the next best activity

in terms of LoD, which was expected as it showed the oxidation peak at 0.34 V. Finally, the NiPc derivative, complex **4**, showed the least activity in terms of LoD, coupled with exhibiting the highest potential. This concludes the investigation and proves that the electronic configuration of the central metal is in fact the most significant factor at play for the catalysis of hydrazine.

Based on the concept that the catalyst must be at a precise potential in order to maximise the catalytic activity, it makes sense that the catalyst should be tuned appropriately and, in the case of Pcs, this is done via the addition of substituents on the periphery of the Pc ligand and choice of the central metal [125,126]. However, what can also be examined is the method of attachment of the catalyst to the surface and the effects the method chosen can have on the catalytic activity of the surface. During this work, an observation was made whereby the **4**-clicked-GCE showed the lack of the typically observed Ni^{II}/Ni^{III} couple seen on electrodes modified via the adsorption method of attachment of the catalyst (Fig. 5.6. (b)) [124,127]. But when complex **4** was adsorbed (not clicked) onto the GCE to form **4**-adsorbed-GCE and scanned repeatedly in 0.2M NaOH (Fig. 5.6. (a)) the Ni^{II}/Ni^{III} couple was observed at ~ 0.45 V. The anodic component of the pair, decreased slightly in intensity and then stabilized. Fig. 5.6. (c) shows one scan from each surface on one axis for comparison. The shapes of the final cyclic voltammograms are very similar to those obtained with electroformed nickel macrocyclic-based films in alkaline aqueous solution, which are also similar to those of $Ni(OH)_2$ on electrodes [124,127]. The formation of the peaks can be explained by the formation of the O-Ni-O oxo bridges in alkaline aqueous solution and are an indication of the transformation of the adsorbed complex **4** into the 'O-Ni-O oxo' bridged forms. The lack of formation of the Ni^{II}/Ni^{III} couple for **4**-clicked-GCE can be attributed to the inability of a hydroxyl group to insert itself between the GCE surface and the nickel at the **4**-clicked-GCE interface, shown schematically in Fig. 5.7. This is because there exists a layer of aryl groups from the grafting step that are covalently bonded to the GCE surface. To this aryl layer complex **4** is bonded as well and hence, there is too much interference for the hydroxyl groups to reach the GCE surface and be oxidized prior to the formation of O-Ni-O as shown in Fig. 5.7(A). In the case of **4**-adsorbed-GCE, Fig. 5.7(B), the oxidation of hydroxide occurs, since there are no aryl groups and the Pc is situated directly on the electrode.

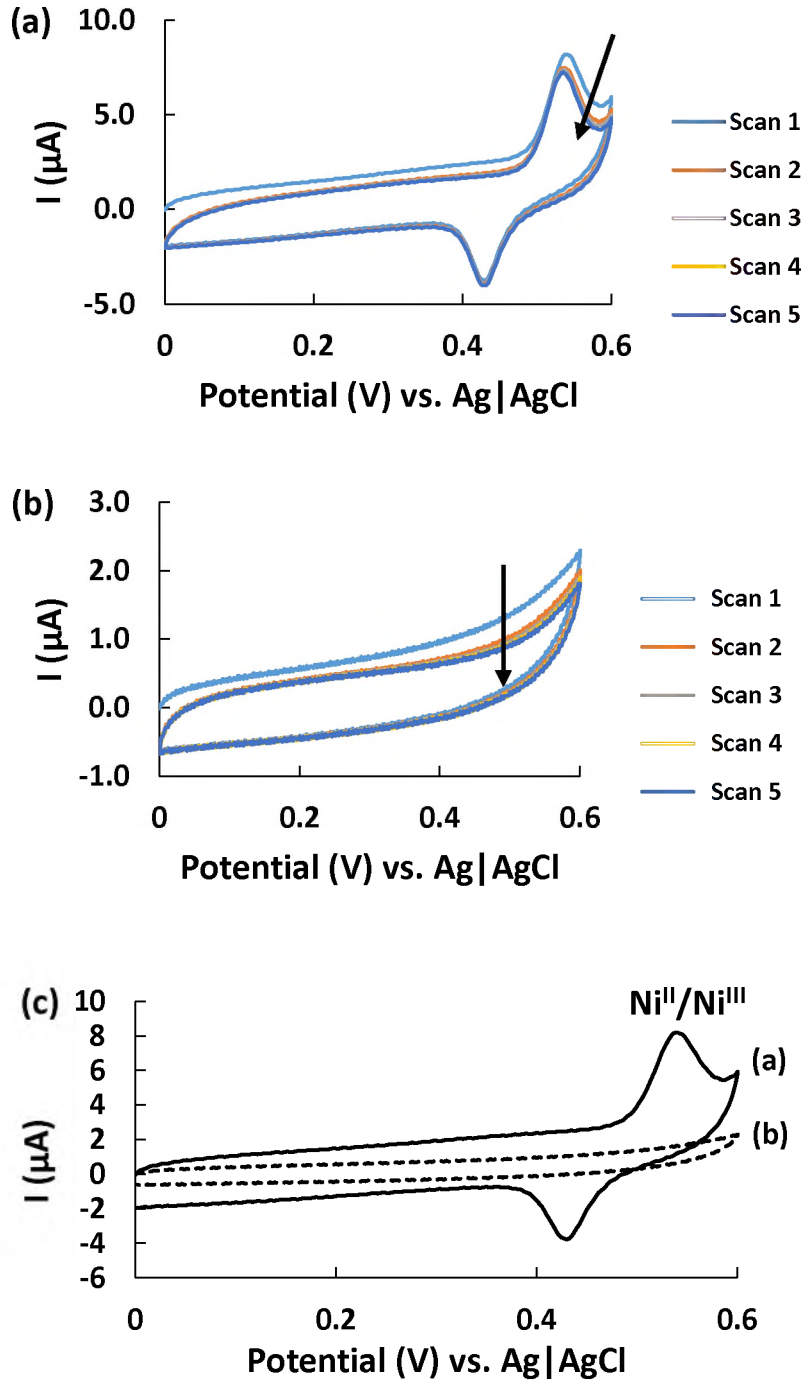

Figure 5.6. Cyclic voltammograms of (a) **4**-adsorbed-GCE showing the presence of the Ni^{II}/Ni^{III} couple, (b) **4**-clicked-GCE showing the absence of the Ni^{II}/Ni^{III} couple, in 0.2M NaOH. Part (c) is shown for comparison sake with **4**-adsorbed-GCE (a) and **4**-clicked-GCE (b) on one axis.

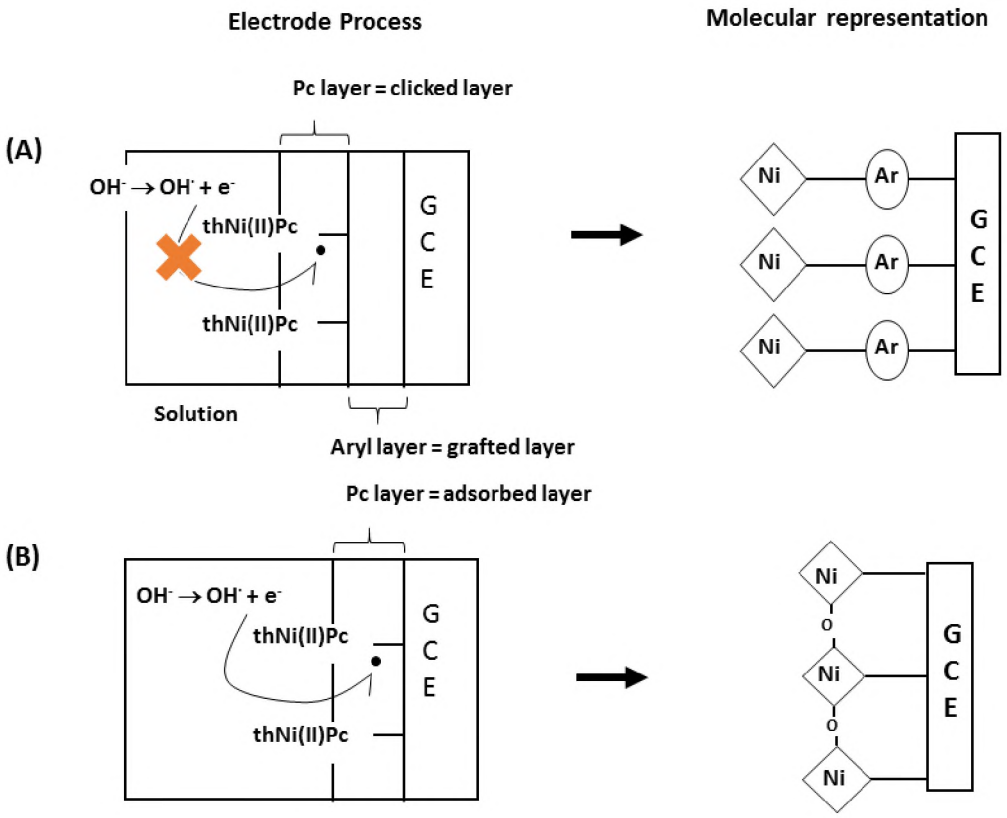

Figure 5.7. A schematic showing the potential explanation as to why a Ni^{II}/Ni^{III} couple is not seen on the **4**-clicked-GCE surface as compared to how this NiPc derivative generates the couple when adsorbed onto the surface.

To bring this into the context of this work, the goal, albeit not exhaustive, was to examine the impact of the graft-then-click modification approach. As most of the literature used to establish the trend discussed is done with the Pcs adsorbed or polymerised, this discussion has been largely speculative in nature. Based on the observations made in the case of the NiPc complex **4** and how the O-Ni-O bridges were potentially not formed, and by the fact that the Pcs are in fact covalently bound to the surface and not bound via electrostatic forces, it is possible that behaviour of the complexes could have changed. This speculation is based on the factor of electron exchange between the electrode surface and the MPc. The passage of electrons via electrostatic forces can be somewhat slower and less consistent than through channels of a covalent bond. So, due to the fact that the Pcs are bonded covalently to the surface, it was hoped the electron transfer capabilities of the catalysts would be improved by the modification approach. However, given the LoDs produced, this was not the case. Instead, there is an improvement, both practically and electrochemically, in terms of consistent catalytic activity and stability. As with the clicked surface, the electrocatalytic reaction

stabilised quickly (5 scans) and was consistent from there onwards. In comparison, the adsorbed variant showed a loss in peak current with each subsequent scan, and effectively no stability was observed.

This observation gives rise to the speculation that the way a surface is modified can impact the behaviour of the catalyst and / or the substrate, and how they interact with each other. It would follow that the attachment of highly conductive materials such as graphene followed by Pc complexes with appropriately tuned electron-withdrawing groups (it seems tetrasulfonated Pcs lead the field [85,90,104,105,112]) would be most apt for this application. It would also seem that the pursuit of this type of surface would be most interesting when click chemistry is also applied. That is not to say that these avenues have not been explored, as many research groups have combined materials to create surfaces with highly modified Pc complexes to better the performance of the catalysts. It is only that the methods of attachment could play a role in the general investigation or pursuit of the optimum system for electrocatalysis of hydrazine.

CHAPTER 6

CONCLUSIONS

CONCLUSIONS

This work illustrated the use of electrochemical grafting and click chemistry for surface modification purposes, in the attachment of electrocatalysts, in the form phthalocyanines, to carbon substrates.

Tetrakis(5-hexyn-oxy) cobalt(II) phthalocyanine (complex **3**) and tetrakis(5-hexyn-oxy) nickel(II) phthalocyanine (complex **4**) were synthesised. The alkyne substituents showed to have minor effects on the UV-vis spectra of the compounds, as well as effects on the electrochemical properties.

This work demonstrated the versatility of 4-azidoaniline as a precursor for the modification of conductive surfaces, in this case glassy carbon electrodes, taking notable advantages of its ability to be further modified through the Sharpless click chemistry reaction. Grafting of the diazonium derivative (**5**) on to bare GCE was achieved. Complexes **2**, **3**, and **4** were covalently linked to the electrode using click chemistry. Using this approach of introducing an azide group to the surface of the electrode through grafting followed by click chemistry was very successful for the grafted electrodes. The process of *in situ* diazotisation of 4-azidoaniline hydrochloride and grafting of the resulting **5** was used at the modification method throughout.

The GCE was studied using electrochemistry, SECM, EIS and XPS to confirm the modification steps. XPS was also used to confirm the attachment of the complexes via click chemistry by tracking the presence or absence of the peak associated with the azide group. While SECM was used to give both two-dimensional and three-dimensional figures of the conductivity of the surfaces. Actual topographic images were generated with the area scan technique of SECM and the surface of the electrodes could be physically visualised via the surfaces conductivity properties.

All three electrode surfaces, **2**-clicked-GCE, **3**-clicked-GCE and **4**-clicked-GCE were successfully used to detect hydrazine, proving the attachment of the complexes and showing their application ability as electrocatalysts. The sensors showed electrocatalytic oxidation of hydrazine with LoDs all in the 10^{-5} M range.

The use of the azido-derivated diazonium molecule **5** opens the doors to important applications and developments devoted to the micro-local functionalisation of electrodes and the implementation of the emerging interfacial click reaction.

A trend was successfully extracted from the work as to what role the central metal plays in the electrocatalysis of hydrazine and based on the two existing mechanisms, each complex was classified as: the FePc mechanism for complexes **2** and **4**, and the CoPc mechanism for complex **3**. The trend of activity was as follows: Co>Mn>Ni, which correlates with literature, and confirms that the central metal governs the activity of the complex.

Future directions for this work could include the usage of a radical scavenger for the azido radical produced in the electro-grafting step, as done by Menanteau *et al.* [25,128], to create a monolayer for click chemistry. This could then be followed by the synthesis of a mono-substituted alkyne MPc, which would then allow for a consistent surface for catalysis. This more consistent surface may then allow for more sensitivity and the redox couples of the MPcs may be visible, which would aid in the challenge of assigning which are responsible for the interaction with hydrazine, when attached to the electrode via covalent methods.

REFERENCES

[1] J. H. Zagal, F. Bedioui, J.-P. Dodelet, Eds. , *N4-Macrocyclic Metal Complexes*, Springer, USA, **2006**.

[2] M. Gouterman, *J. Mol. Spectrosc.* **1961**, *6*, 138–163.

[3] T. Nyokong, M. J. Stillman, in *Phthalocyanines: Properties and Applications* (Eds.: C.C. Leznoff, A.B.P. Lever), VCH, New York, **1989**.

[4] O. V Dolotova, N. I. Bundina, O. L. Kaliya, E. A. Lukyanets, *J. Porphyr. Phthalocyanines* **1997**, *1*, 355–366.

[5] T. Mugadza, T. Nyokong, *Electrochim. Acta* **2010**, *55*, 6049–6057.

[6] J. Obirai, T. Nyokong, *Electrochim. Acta* **2005**, *50*, 3296–3304.

[7] B. Agboola, K. I. Ozoemena, T. Nyokong, *Electrochim. Acta* **2006**, *51*, 4379–4387.

[8] J. Obirai, T. Nyokong, *Electrochim. Acta* **2005**, *50*, 5427–5434.

[9] B. Agboola, K. I. Ozoemena, P. Westbroek, T. Nyokong, *Electrochim. Acta* **2007**, *52*, 2520–2526.

[10] N. Sehlotho, M. Durmuş, V. Ahsen, T. Nyokong, *Inorg. Chem. Commun.* **2008**, *11*, 479–483.

[11] A. I. Adebayo, T. Nyokong, *Polyhedron* **2009**, *28*, 2831–2838.

[12] F. Matemadombo, S. Griveau, F. Bedioui, T. Nyokonga, *Electroanalysis* **2008**, *20*, 1863–1872.

[13] D. Dini, M. Hanack, in *The Porphyrin Handbook: Properties and Materials* (Eds.: K.M. Kadish, K.M. Smith, R. Guilard), Academic Press, Amsterdam, **2003**, pp. 1–36.

[14] E. Ben-Hur, W.-S. Chan, in *The Porphyrin Handbook: Applications of Phthalocyanines* (Eds.: K.M. Kadish, K.M. Smith, R. Guilard), Academic Press, Amsterdam, **2003**, pp. 1–35.

[15] S. R. Nxele, P. Mashazi, T. Nyokong, *Electroanalysis* **2015**, *27*, 2468–2478.

[16] K. Kasuga, M. Tsutsui, *Coord. Chem. Rev.* **1980**, *32*, 67–95.

[17] V. N. Nemykin, E. A. Lukyanets, in *Handbook of Porphyrin Science* (Eds.: K.M. Kadish, K.M. Smith, R. Guilard), World Scientific Publishing Company, Singapore, **2010**, pp. 1–323.

[18] T. Nyokong, H. Isago, *J. Porphyr. Phthalocyanines* **2004**, *8*, 1083–1090.

[19] J. Mack, M. J. Stillman, N. Kobayashi, *Coord. Chem. Rev.* **2007**, *251*, 429–453.

[20] T. Furuyama, K. Satoh, T. Kushiya, N. Kobayashi, *J. Am. Chem. Soc.* **2014**, *136*, 765–776.

[21] M. Delamar, R. Hitmi, J. Pinson, J. M. Saveant, *J. Am. Chem. Soc.* **1992**, *114*, 5883–5884.

[22] P. Allongue, M. Delamar, B. Desbat, O. Fagebaume, R. Hitmi, J. Pinson, J. Save, *J. Am. Chem. Soc.* **1997**, *7863*, 201–207.

[23] C. Saby, B. Ortiz, G. Y. Champagne, D. Bélanger, *Langmuir* **1997**, *13*, 6805–6813.

[24] D. Bélanger, J. Pinson, *Chem. Soc. Rev.* **2011**, *40*, 3995–4048.

[25] T. Menanteau, E. Levillain, T. Breton, *Chem. Mater.* **2013**, *25*, 2905–2909.

[26] P. Doppelt, G. Hallais, J. Pinson, F. Podvorica, S. Verneyre, *Chem. Mater.* **2007**, *19*, 4570–4575.

[27] D. Evrard, F. Lambert, C. Policar, V. Balland, B. Limoges, *Chem. - A Eur. J.* **2008**, *14*, 9286–9291.

[28] A. Adenier, N. Barré, E. Cabet-Deliry, A. Chaussé, S. Griveau, F. Mercier, J. Pinson, C. Vautrin-Ul, *Surf. Sci.* **2006**, *600*, 4801–4812.

[29] S. Griveau, D. Mercier, C. Vautrin-Ul, A. Chaussé, *Electrochem. commun.* **2007**, *9*, 2768–2773.

[30] S. Baranton, D. Bélanger, *Electrochim. Acta* **2008**, *53*, 6961–6967.

[31] J. K. Kariuki, M. T. McDermott, *Langmuir* **2001**, *17*, 5947–5951.

[32] R. Huisgen, *Angew. Chemie* **1963**, *75*, 604–637.

[33] Z. Kanat, H. Dinçer, *Dalt. Trans.* **2014**, *43*, 8654–8663.

[34] H. Dinçer, H. Mert, E. Çalışkan, G. Y. Atmaca, A. Erdoğmuş, *J. Mol. Struct.* **2015**, *1102*, 190–196.

[35] D. Quinton, E. Antunes, S. Griveau, T. Nyokong, F. Bedioui, *Inorg. Chem. Commun.* **2011**, *14*, 330–332.

[36] A. Wichmann, G. Schnurpfeil, J. Backenköhler, L. Kolke, V. A. Azov, D. Wöhrle, M. Bäumer, A. Wittstock, *Tetrahedron* **2014**, *70*, 6127–6133.

[37] Y. Yilmaz, J. Mack, M. Soenmez, T. Nyokong, *J. Porphyr. Phthalocyanines* **2014**, *18*, 251–258.

[38] Y. Yilmaz, M. Kasim Şener, I. Erden, U. Avciata, *Polyhedron* **2009**, *28*, 3419–3424.

[39] D. K. Muli, B. L. Carpenter, M. Mayukh, R. A. Ghiladi, D. V. McGrath, *Tetrahedron Lett.* **2015**, *56*, 3541–3545.

[40] X. Chen, J. Thomas, P. Gangopadhyay, R. A. Norwood, N. Peyghambarian, D. V. McGrath, *J. Am. Chem. Soc.* **2009**, *131*, 13840–13843.

[41] M. Li, E. Khoshdel, D. M. Haddleton, *Polym. Chem.* **2013**, *4*, 4405–4411.

[42] B. N. Şen, H. Mert, H. Dinçer, A. Koca, *Dye. Pigment.* **2014**, *100*, 1–10.

[43] X. Chen, C. W. Lu, Y. Huang, D. V. McGrath, *Tetrahedron* **2015**, *71*, 9154–9160.

[44] A. Fashina, E. Amuhaya, T. Nyokong, *Spectrochim. Acta - Part A Mol. Biomol. Spectrosc.* **2015**, *140*, 256–264.

[45] Y. Bandera, M. K. Burdette, J. A. Shetzline, R. Jenkins, S. E. Creager, S. H. Foulger, *Dye. Pigment.* **2016**, *125*, 72–79.

[46] U. Hahn, T. Torres, *J. Porphyr. Phthalocyanines* **2011**, *15*, 364–372.

[47] K. H. Le Ho, L. Rivier, B. Jousselme, P. Jégou, A. Filoramo, S. Campidelli, *Chem. Commun. (Camb).* **2010**, *46*, 8731–8733.

[48] S. Sari, M. Durmuş, M. Bulut, *Tetrahedron Lett.* **2016**, *57*, 1124–1128.

[49] M. Mayukh, C. W. Lu, E. Hernandez, D. V. McGrath, *Chem. - A Eur. J.* **2011**, *17*, 8472–8478.

[50] V. Novakova, K. Kopecky, M. Miletin, J. Ivincova, P. Zimcik, *J. Porphyr. Phthalocyanines* **2011**, *15*, 1062–1069.

[51] Y. Zorlu, F. Dumoulin, D. Bouchu, V. Ahsen, D. Lafont, *Tetrahedron Lett.* **2010**, *51*, 6615–6618.

[52] H. Dinçer, H. Mert, B. N. Şen, A. Dağ, S. Bayraktar, *Dye. Pigment.* **2013**, *98*, 246–254.

[53] J. Wang, *Analytical Electrochemistry*, Wiley-VCH, New York, **2000**.

[54] C. Brett, A. Brett, *Electrochemistry: Principles, Methods, and Applications*, Oxford University Press, Oxford, **1993**.

[55] W. E. Van der Linden, J. W. Dieker, *Anal. Chim. Acta* **1980**, *119*, 1–24.

[56] M. Coates, T. Nyokong, *J. Electroanal. Chem.* **2012**, *687*, 111–116.

[57] S. Baranton, D. Bélanger, *J. Phys. Chem. B* **2005**, *109*, 24401–24410.

[58] C. Cougnon, F. Gohier, D. Belanger, J. Mauzeroll, *Angew. Chemie - Int. Ed.* **2009**, *48*, 4006–4008.

[59] H. C. Kolb, M. G. Finn, K. B. Sharpless, *Angew. Chemie - Int. Ed.* **2001**, *40*, 2004–2021.

[60] V. V. Rostovtsev, L. G. Green, V. V. Fokin, K. B. Sharpless, *Angew. Chemie - Int. Ed.* **2002**, *41*, 2596–2599.

[61] L. Liang, D. Astruc, *Coord. Chem. Rev.* **2011**, *255*, 2933–2945.

[62] J. F. Lutz, Z. Zarafshani, *Adv. Drug Deliv. Rev.* **2008**, *60*, 958–970.

[63] B. K. Yoo, S. W. Joo, *J. Colloid Interface Sci.* **2007**, *311*, 491–496.

[64] V. D. Bock, H. Hiemstra, J. H. Van Maarseveen, *European J. Org. Chem.* **2006**, 51–68.

[65] T. Lummerstorfer, H. Hoffmann, *J. Phys. Chem. B* **2004**, *108*, 3963–3966.

[66] N. K. Devaraj, G. P. Miller, W. Ebina, B. Kakaradov, J. P. Collman, E. T. Kool, C. E. D. Chidsey, *J. Am. Chem. Soc.* **2005**, *127*, 8600–8601.

[67] J. P. Collman, N. K. Devaraj, A. Eberspacher, C. E. D. Chidsey, *Langmuir* **2006**, *22*, 2457–2464.

[68] J. P. Collman, N. K. Devaraj, C. E. D. Chidsey, *Langmuir* **2004**, *20*, 1051–1053.

[69] J. G. Lee, K. Il Choi, H. Yeong Koh, Y. Kim, Y. Kang, Y. Seo Cho, *Synthesis (Stuttg).* **2001**, 81–84.

[70] H. Zhang, S. Shuang, L. Sun, A. Chen, Y. Qin, C. Dong, *Microchim. Acta* **2014**, *181*, 189–196.

[71] A. J. Bard, L. R. Faulkner, *Electrochemical Methods: Fundamentals and Applications*, Wiley, New York, **2001**.

[72] E. Barsoukov, J. R. Macdonald, Eds. , *Impedance Spectroscopy: Theory, Experiment, and Applications*, John Wiley & Sons, Inc., Hoboken, **2005**.

[73] P. Mashazi, T. Nyokong, *Microchim. Acta* **2010**, *171*, 321–332.

[74] J. F. Watts, J. Wolstenholme, *An Introduction to Surface Analysis by XPS and AES*, John Wiley & Sons, Ltd., Chichester, UK, **2003**.

[75] R. K. Schulze, D. C. Boyd, J. F. Evans, W. L. Gladfelter, *J. Vac. Sci. Technol. A Vacuum, Surfaces, Film.* **1990**, *8*, 2338–2343.

[76] A. Devadoss, C. E. D. Chidsey, *J. Am. Chem. Soc.* **2007**, *129*, 5370–5371.

[77] E. C. Landis, R. J. Hamers, *Chem. Mater.* **2009**, *21*, 724–730.

[78] S. Prakash, T. M. Long, J. C. Selby, J. S. Moore, M. A. Shannon, *Anal. Chem.* **2007**, *79*, 1661–1667.

[79] M. V. Mirkin, W. Nogala, J. Velmurugan, Y. Wang, *Phys. Chem. Chem. Phys.* **2011**, *13*, 21196.

[80] A. J. Bard, G. Denuault, C. Lee, D. Mandler, D. O. Wipf, *Acc. Chem. Res.* **1990**, *23*, 357–363.

[81] J. Kwak, A. J. Bard, *Anal. Chem.* **1989**, *61*, 1221–1227.

[82] A. J. Bard, F. F. Fan, J. Kwak, O. Lev, *Anal. Chem.* **1989**, *61*, 132–138.

[83] A. J. Bard, F. R. Fan, D. T. Pierce, P. R. Unwin, D. O. Wipf, F. Zhou, *Science* **1991**, *254*, 68–74.

[84] S. Griveau, S. Aroua, D. Bediwy, R. Cornut, C. Lefrou, F. Bedioui, *J. Electroanal. Chem.* **2010**, *647*, 93–96.

[85] J. H. Zagal, S. Griveau, J. F. Silva, T. Nyokong, F. Bedioui, *Coord. Chem. Rev.* **2010**, *254*, 2755–2791.

[86] D. A. Geraldo, C. A. Togo, J. Limson, T. Nyokong, *Electrochim. Acta* **2008**, *53*, 8051–8057.

[87] J. R. Latendresse, G. B. Marit, E. H. Vernot, C. C. Haun, C. D. Flemming, *Toxicol. Sci.* **1995**, *27*, 33–48.

[88] K. Bando, T. Kunimatsu, J. Sakai, J. Kimura, H. Funabashi, T. Seki, T. Bamba, E. Fukusaki, *J. Appl. Toxicol.* **2011**, *31*, 524–535.

[89] F. Cardulla, *J. Chem. Educ.* **1983**, *60*, 505–508.

[90] F. S. Damos, R. de Cassia Silva Luz, A. A. Tanaka, in *Electrochemistry of N4 Macrocyclic Metal Complexes* (Eds.: J.H. Zagal, F. Bedioui), Springer International Publishing, Cham, **2016**, pp. 201–224.

[91] A. G. Gürek, Ö. Bekaroğlu, *J. Chem. Soc. Dalt. Trans.* **1994**, *9*, 1419–1423.

[92] T. Breton, D. Bélanger, *Langmuir* **2008**, *24*, 8711–8718.

[93] M. Durmuş, S. Yeşilot, V. Ahsen, *New J. Chem.* **2006**, *30*, 675–678.

[94] T. Nyokong, in *Functional Phthalocyanine Molecular Materials* (Ed.: J. Jiang), Springer Berlin Heidelberg, Berlin, Heidelberg, **2010**, pp. 45–87.

[95] J. Obirai, N. P. Rodrigues, F. Bedioui, T. Nyokong, *J. Porphyr. Phthalocyanines* **2003**, *7*, 508–520.

[96] S. Baranton, C. Coutanceau, C. Roux, F. Hahn, J. M. Léger, *J. Electroanal. Chem.* **2005**, *577*, 223–234.

[97] J. Lyskawa, D. Bélanger, *Chem. Mater.* **2006**, *18*, 4755–4763.

[98] F. Matemadombo, P. Westbroek, T. Nyokong, *Electrochim. Acta* **2007**, *53*, 480–486.

[99] D. C. Boyd, R. T. Haasch, D. R. Mantell, R. K. Schulze, J. F. Evans, W. L. Gladfelter, *Chem. Mater.* **1989**, *1*, 119–124.

[100] A. E. Daugaard, S. Hvilsted, T. S. Hansen, N. B. Larsen, *Macromolecules* **2008**, *41*, 4321–4327.

[101] J. Francisco Silva, S. Griveau, C. Richard, J. H. Zagal, F. Bedioui, *Electrochem. commun.* **2007**, *9*, 1629–1634.

[102] Z. P. Demko, K. B. Sharpless, *Angew. Chemie - Int. Ed.* **2002**, *41*, 2113–2116.

[103] M. Coates, Characterisation of Surfaces Modified through Self-Assembled Monolayers and Click Chemistry, Rhodes University, **2013**.

[104] J. Zagal, E. Muñoz, S. Ureta-Zañartu, *Electrochim. Acta* **1982**, *27*, 1373–1377.

[105] J. H. Zagal, S. Lira, S. Ureta-Zañartu, *J. Electroanal. Chem.* **1986**, *210*, 95–110.

[106] E. Trollund, P. Ardiles, **2000**, *19*, 2303–2312.

[107] C. Linares, D. Geraldo, M. Paez, J. H. Zagal, *J. Solid State Electrochem.* **2003**, *7*, 626–631.

[108] J. H. Zagal, F. Bedioui, Eds. , *Electrochemistry of N4 Macrocyclic Metal Complexes*, Springer International Publishing, Cham, **2016**.

[109] A. Salimi, K. Abdi, *Talanta* **2004**, *63*, 475–483.

[110] J. M. Zen, A. Senthil Kumar, M. R. Chang, *Electrochim. Acta* **2000**, *45*, 1691–1699.

[111] C. A. Caro, F. Bedioui, J. H. Zagal, *Electrochim. Acta* **2002**, *47*, 1489–1494.

[112] J. Zagal, S. Ureta-Zanartu, *J. Electrochem. Soc.* **1982**, *129*, 2242–2247.

[113] E. Sabatani, I. Rubinstein, R. Maoz, J. Sagiv, *J. Electroanal. Chem. Interfacial Electrochem.* **1987**, *219*, 365–371.

[114] V. Lakshminarayanan, U. Kumar Sur, *Pramana - J. Phys.* **2003**, *61*, 361–371.

[115] Z. Galus, *Fundamentals of Electrochemical Analysis*, Ellis Horwood Press, New York, **1991**.

[116] J. H. Zagal, *J. Electroanal. Chem.* **1980**, *109*, 389–393.

[117] C. das D. C. Conceição, R. C. Faria, O. Fatibello-Filho, A. A. Tanaka, *Anal. Lett.* **2008**, *41*, 1010–1021.

[118] E. F. Perez, G. D. O. Neto, A. A. Tanaka, L. T. Kubota, *Electroanalysis* **1998**, *10*, 111–115.

[119] T. J. Mafatle, T. Nyokong, *J. Electroanal. Chem.* **1996**, *408*, 213–218.

[120] K. I. Ozoemena, T. Nyokong, *Talanta* **2005**, *67*, 162–168.

[121] R. Taube, *Pure Appl. Chem.* **1974**, *38*, 427–438.

[122] F. Tasca, F. J. Recio, R. Venegas, D. A. Geraldo, M. Sancy, J. H. Zagal, *Electrochim. Acta* **2014**, *140*, 314–319.

[123] K. I. Ozoemena, *Sensors* **2006**, *6*, 874–891.

[124] S. Khene, K. Lobb, T. Nyokong, *Electrochim. Acta* **2010**, *56*, 706–716.

[125] M. Villagrán, F. Caruso, M. Rossi, J. H. Zagal, J. Costamagna, *Eur. J. Inorg. Chem.* **2010**, *2010*, 1373–1380.

[126] U. Isci, F. Dumoulin, V. Ahsen, A. B. Sorokin, *J. Porphyr. Phthalocyanines* **2010**, *14*, 324–334.

[127] V. Chauke, F. Matemadombo, T. Nyokong, *J. Hazard. Mater.* **2010**, *178*, 180–186.

[128] T. Menanteau, M. Dias, E. Levillain, A. J. Downard, T. Breton, *J. Phys. Chem. C* **2016**, *120*, 4423–4429.